Characterization of a Unique Tomaymycin–d(CICGAATTCICG)$_2$ Adduct Containing Two Drug Molecules per Duplex by NMR, Fluorescence, and Molecular Modeling Studies†

F. Leslie Boyd,‡ Diana Stewart,§ William A. Remers,‖ Mary D. Barkley,⊥ and Laurence H. Hurley*,‡

Department of Chemistry and Drug Dynamics Institute, College of Pharmacy, University of Texas at Austin, Austin, Texas 78712, Department of Medicinal Chemistry, College of Pharmacy, University of Arizona, Tucson, Arizona 85721, and Department of Chemistry, Louisiana State University, Baton Rouge, Louisiana 70803

Received July 26, 1989; Revised Manuscript Received October 23, 1989

ABSTRACT: Tomaymycin is a member of the pyrrolo[1,4]benzodiazepine [P(1,4)B] antitumor antibiotic group. This antibiotic is proposed to react with the exocyclic 2-amino group (N2) of guanine to form a covalent adduct that lies snugly within the minor groove of DNA. While DNA-footprinting experiments using methidiumpropyl-EDTA have revealed the favored bonding sequences for tomaymycin and related drugs on DNA, the stereochemistry at the covalent bonding site (C-11) and orientation in the minor groove were not established by these experiments. In previous studies using a combined fluorescence, high-field NMR, and molecular modeling approach, we have shown that for tomaymycin there are two diastereomeric species (11*R* and 11*S*) on both calf thymus DNA and d(ATGCAT)$_2$. Although we were able to infer the identity (stereochemistry at C-11 and orientation in the minor groove) of the two species on d(ATGCAT)$_2$ by high-field NMR and fluorescence studies, in combination with molecular mechanics calculations, definitive experimental evidence was lacking. We have designed and synthesized a self-complementary 12-mer [d(CICGAATTCICG)$_2$] based on the Dickerson dodecamer [d(CGCGAATTCGCG)$_2$] that bonds identically two tomaymycin molecules, each having a defined orientation and stereochemistry. Thus the bis(tomaymycin)–12-mer adduct maintains the self-complementarity of the original duplex molecule. Two-dimensional proton *J*-correlated spectroscopy (COSY) of the bis(tomaymycin)–d(CICGAATTCICG)$_2$ adduct (I = inosine) unequivocally shows that C-11 of tomaymycin covalently bonds through N2 of guanine with an 11*S* stereochemistry in the sequence 5′-CGA-3′. Fluorescence studies confirm the "*S*" stereochemistry at C-11, and two-dimensional proton nuclear Overhauser (NOESY) experiments assign the orientation of the drug molecule in the minor groove of DNA, i.e., with the aromatic ring of tomaymycin to the 3′ side of covalently modified guanine. Molecular modeling experiments with AMBER are consistent with the identification of the species of tomaymycin (11*S* with 3′ orientation) bound to the 12-mer. This species and the other 11*S* species are favored over the two 11*R* species due to a combination of steric and electrostatic interactions. Analysis of two-dimensional COSY and NOESY experiments on the bis(tomaymycin)–d(CICGAATTCICG)$_2$ adducts reveals minimal effect of covalent bonding on local helix structure. From these experiments the modest but most pronounced distortion is at the deoxyribose attached to the modified guanine and both the phosphate and adjacent deoxyribose to the 5′ side. The distortion of this phosphate between the covalently modified guanine and the 5′ nucleoside is supported by its downfield-shifted phosphorus NMR resonance signal. The discrepancy between the pairs of most energetically favored species of tomaymycin–DNA adducts on d(ATGCAT)$_2$ and the 12-mer is explained by examining individual drug–nucleotide interactions. The results presented in this study together with previous investigations show that the orientation of the drug molecule in the minor groove, and stereochemistry at the covalent linkage site, is dependent upon both the flanking sequence and drug structure. This conclusion mandates caution be used in rationalizing the biochemical and biological effects of P(1,4)B bonding to DNA until precise structural information is established.

Tomaymycin and anthramycin are members of the P(1,4)B[1] antitumor–antibiotic group (Hurley, 1977; Hurley & Needham-VanDevanter, 1986; Remers, 1988). These drugs are proposed to react via the C-11, N-10 imine **2** to form the unique covalent adduct **3** through the exocyclic 2-amino group (N2) of guanine (Figure 1) (Petrusek et al., 1982; Barkley et al., 1986). There is an excellent correlation between both in vivo and in vitro cytotoxic potency of the P(1,4)Bs and their ability to form covalent adducts through N2 of guanine on DNA for a variety of natural and synthetic compounds (Hurley et al., 1988; Thurston & Hurley, 1983). DNA-footprinting experiments with MPE (Hertzberg et al., 1986)

† This work was supported by grants from the NIH (GM-35009), the National Cancer Institute (CA-49751 and CA-37798), the Welch Foundation, and the Texas Advanced Technology Program.

* To whom correspondence should be addressed.
‡ Drug Dynamics Institute, University of Texas at Austin.
§ Department of Chemistry, University of Texas at Austin.
‖ University of Arizona.
⊥ Louisiana State University.

[1] Abbreviations: P(1,4)B, pyrrolo[1,4]benzodiazepine; MPE, methidiumpropylethylenediaminetetraacetic acid; exo-III, exonuclease III; COSY, correlated spectroscopy; NOE, nuclear Overhauser effect; NOESY, nuclear Overhauser effect spectroscopy; I, inosine; TME, tomaymycin 11-methyl ether; XP, xeroderma pigmentosum; TSP, 3-(trimethylsilyl)propionic-*2,2,3,3-d*$_4$ acid sodium salt.

0006-2960/90/0429-2387$02.50/0

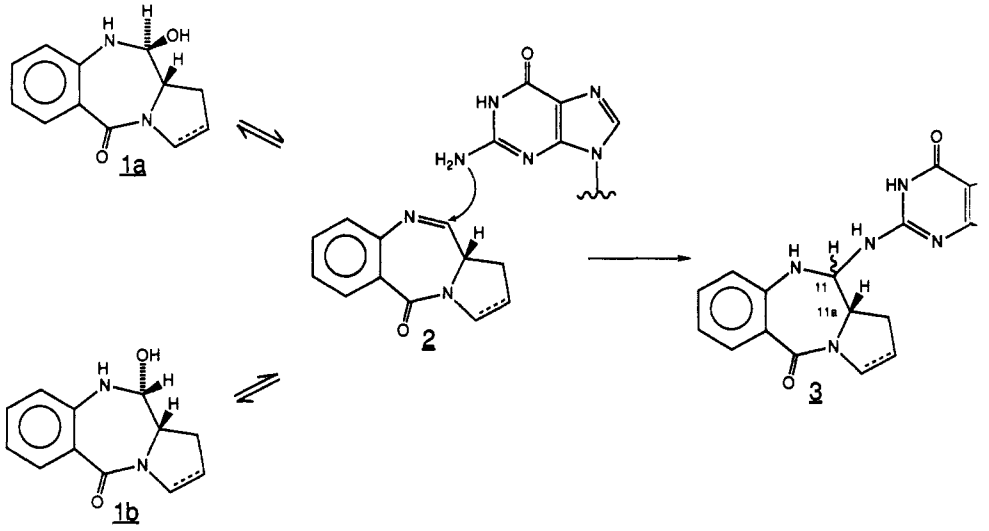

FIGURE 1: Proposed reaction of the P(1,4)Bs with DNA (Barkley et al., 1986).

and an exo-III stop assay (Hurley et al., 1988) concur that the most favored sequences for covalent bonding are 5′-PuGPu and the least favored are 5′-PyGPy, with 5′-PyGPu and 5′-PuGPy sequences of intermediate bonding reactivity.

Tomaymycin (**4**) and anthramycin (**5**) (Figure 2) both have a right-handed twist along the length of the molecule (Arora, 1981; Mostad et al., 1978) and are predicted by molecular modeling studies (Petrusek et al., 1982; Remers et al., 1986; Rao et al., 1986; Zakrzewska & Pullman, 1986) to be accommodated within the minor groove of DNA without large distortion of the DNA helix.[2] While DNA-sequencing experiments using MPE or exo-III reveal the favored covalent bonding sequences for anthramycin and tomaymycin, they are blind to important questions relating to the orientation of the drug molecule in the minor groove and the stereochemistry at the covalent linkage site between C-11 of the P(1,4)Bs and N2 of guanine. In order to address these questions, we have examined, by a combined high-field NMR, fluorescence, and molecular modeling approach, short oligomers such as d-$(ATGCAT)_2$ that contain a single drug bonding site. For anthramycin on $d(ATGCAT)_2$ a single adduct has been demonstrated (Graves et al., 1985) in which the aromatic ring of the drug is oriented to the 3′ side of the covalently modified guanine and most likely has an 11*S* linkage stereochemistry (Boyd et al., 1990). For tomaymycin, fluorescence studies first suggested that tomaymycin can bond to calf thymus DNA with either the *R* or *S* configuration at C-11 (Barkley et al., 1986). With $d(ATGCAT)_2$ a combined fluoresence, high-field NMR, and molecular modeling study showed two species of tomaymycin bound to the oligomer, each having the opposite stereochemistry at C-11 (Cheatham et al., 1988). Although not definitive, the two species bound to this duplex were tentatively identified as the 11*S* and 11*R* diastereomers with the drug molecule oriented to either the 3′ or 5′ direction, respectively. In contrast, results from proton NMR experiments with other oligomers [$d(TTCGAA)_2$ and $d(AAGCTT)_2$] showed predominantly one species of tomaymycin bound to each of these oligomers (Cheatham and Boyd, unpublished results).

The Dickerson dodecamer [$d(CGCGAATTCGCG)_2$] (Drew et al., 1981) was used as a starting point to design a self-complementary 12-mer sequence that would bond two tomaymycin molecules, each with the same defined orientation and stereochemistry. This dodecamer has three internal guanines (underlined in the 12-mer) that are potential tomaymycin covalent bonding sites (the terminal guanine is unlikely to be a bonding site). Two of these guanines were replaced with inosine, leaving only the guanine in the CGA sequence as a potential tomaymycin bonding site. Inosine differs from guanine only in that it lacks the exocyclic 2-amino group. In the inosine-disubstituted dodecamer [d(CICGA-ATTCICG)$_2$] the remaining tomaymycin-reactive guanine is contained within the sequence (5′-CGA) that is predicted from previous unpublished studies from our laboratories (see above) to bond predominantly one species of tomaymycin. In the present study we provide evidence for this assumption and determine independently by fluorescence and high-field NMR the stereochemistry at the covalent linkage site. NOESY experiments assign the orientation of tomaymycin in the minor groove of DNA. We also show that there is a very modest change in local conformation of DNA upon adduct formation. The results of molecular modeling using the AMBER molecular mechanics program are in good agreement with these results. These calculations provide insight into the molecular interactions which favor the experimentally determined species on this 12-mer. It has long been assumed that the P(1,4)Bs form covalent adducts through N2 of guanine (Hurley, 1977). The present proton NMR results provide the first *direct* evidence for covalency between N2 of guanine and C-11 of a P(1,4)B.

Materials and Methods

Chemicals. (11*R*,11a*S*)-TME was generous gift from Dr. Kohsaka of Fujisawa Pharmaceuticals. d(CICGAATT-CICG)$_2$ was prepared by The Midland Certified Reagent Co. by solid-phase phosphoramidite chemistry.

Purification of d(CICGAATTCICG)$_2$. d(CICGAATT-CICG)$_2$ was purified in-house on a Machery-Nagel Nucleogen-DEAE 60-7 HPLC column with an increasing gradient to 1 M NaCl in 15 mM sodium phosphate and 20% acetonitrile/aqueous buffer, pH 6.8.

Preparation of the Bis(tomaymycin)–d(CICGAATTCICG)$_2$ Adduct. (A) NMR Experiments. The bis(tomaymycin)–12-mer adduct was prepared by adding ~4 mg of the solid (11*R*,11a*S*)-TME to ~250 A_{260} units of the self-complementary oligomer in 600 μL of 10 mM NaH_2PO_4, 100 mM NaCl, and 0.01 mM EDTA-buffered D_2O at pH 6.8. The mixture was lyophilized to dryness and reconstituted in 1 mL

[2] For anthramycin covalently bound to $d(ATGCAT)_2$, Zakrzewska and Pullman (1986) predict a B- toward an A-type transition of the DNA.

Table I

(A) Comparison of the Base Proton NMR Chemical Shift Assignments (ppm) and T_1 Relaxation Times of Nonexchangeable and Imino Protons of d(CICGAATTCICG)$_2$ and the Bis(tomaymycin)–d(CICGAATTCICG)$_2$ Adduct in D_2O at 24 °C

assignment	d(CICGA-ATTCICG)$_2$, δ	bis(tomaymycin)–d(CICGAATT-CICG)$_2$ δ	bis(tomaymycin)–d(CICGAATT-CICG)$_2$ Δδ	assignment	d(CICGAATTCICG)$_2$, δ	bis(tomaymycin)–d(CICGAATTCICG)$_2$ δ	bis(tomaymycin)–d(CICGAATTCICG)$_2$ Δδ
				Aromatic Protons			
^{1}C H6	7.62	7.58	−0.04	^{12}G H8	7.89	7.84	−0.05
^{2}I H8	8.30	8.20	−0.10	^{1}C H5	5.90	5.82	−0.08
^{3}C H6	7.18	7.29	+0.11	^{2}I H2	7.85 (4.19 ± 0.08)	7.80 (5.06 ± 0.17)	−0.05 (+0.87)
^{4}G H8	7.81	7.62	−0.19	^{3}C H5	5.26	5.22	−0.04
^{5}A H8	8.10	7.86	−0.24	^{5}A H2	7.15 (3.10 ± 0.06)	7.24 (4.51 ± 0.15)	+0.09 (+1.41)
^{6}A H8	8.10	7.95	−0.25	^{6}A H2	7.57 (3.75 ± 0.09)	7.65 (5.19 ± 0.18)	+0.08 (+1.44)
^{7}T H6	7.07	7.27	+0.20	^{7}T Me	1.22	1.15	−0.07
^{8}T H6	7.33	7.07	−0.26	^{8}T Me	1.50	1.49	−0.01
^{9}C H6	7.47	7.24	−0.23	^{9}C H5	5.62	5.32	−0.30
^{10}I H8	8.25	8.06	−0.19	^{10}I H2	7.66 (3.66 ± 0.06)	7.22 (3.86 ± 0.09)	−0.44[a] (+0.20)
^{11}C H6	7.21	7.18	−0.03	^{11}C H5	5.35	5.22	−0.13
				Imino Protons (10 °C)			
^{1}C–^{12}G	12.70	12.80	+0.10	^{4}G–^{9}C	12.40	12.42	+0.02
^{2}I–^{11}C	15.38	15.41	+0.03	^{5}A–^{8}T	13.55	14.02	+0.47[a]
^{3}C–^{10}I	15.17	15.12	−0.05	^{6}A–^{7}T	13.60	13.60	−0.00

(B) Comparison of the Deoxyribofuranose Proton Chemical Shift Assignments (ppm) of d(CICGAATTCICG)$_2$ and the Bis(tomaymycin)–d(CICGAATTCICG)$_2$ Adduct

	deoxyribose protons														
	H1′			H2′			H2″			H3′			H4′		
assignment	12-mer	T-12-mer	Δδ	12-mer	T-12-mer	Δδ	12-mer	T-12-mer	Δδ	12-mer	T-12-mer	Δδ	12-mer	T-12-mer	Δδ
^{1}C	5.59	5.55	−0.04	1.96	1.90	−0.06	2.35	2.30	−0.05	4.61	4.62	+0.01	4.03	4.01	−0.02
^{2}I	6.15	6.18	+0.03	2.72	2.65	−0.07	2.85	2.82	−0.03	4.92	4.93	+0.01	4.42	4.38	−0.04
^{3}C	5.67	5.39	−0.28	1.58	2.06	+0.48	2.14	2.29	+0.15	4.67	4.75	+0.08	4.03	4.16	+0.13
^{4}G	5.26	6.00	+0.74[a]	2.63	2.43	−0.20	2.67	2.80	+0.13	4.88	4.92	+0.04	4.28	4.36	+0.08
^{5}A	5.94	5.75	−0.19	2.65	2.44	−0.21	2.89	2.55	−0.34	4.98	4.88	−0.10	4.40	4.24[b]	−0.16
^{6}A	6.08	5.80	−0.28	2.60	2.21	−0.39	2.88	2.79	−0.09	4.92	4.70	−0.22	4.42	3.92	−0.50
^{7}T	5.83	5.98	+0.15	1.95	1.95	+0.00	2.53	2.60	+0.07	4.71	4.85	+0.14	4.09	4.24[b]	+0.15
^{8}T	6.04	6.05	+0.01	2.12	2.15	+0.03	2.51	2.57	+0.06	4.82	4.89	+0.07	4.12	4.20[b]	+0.08
^{9}C	5.46	5.72	+0.26	2.05	1.80	−0.25	2.35	2.14	−0.21	4.79	4.84	+0.05	4.12	4.20[b]	+0.08
^{10}I	6.13	5.78	−0.35	2.70	2.55	−0.15	2.86	2.55	−0.31	4.94	4.81	−0.13	4.37	4.24	−0.13
^{11}C	5.78	5.83	+0.05	1.64	1.52	−0.12	2.20	2.15	−0.05	4.72	4.69	−0.03	4.18	3.81	−0.37
^{12}G	6.09	6.09	0.00	2.24	2.29	−0.05	2.61	2.55	−0.06	4.57	4.61	+0.04	4.15	4.00	−0.15

[a] Δδ underlined are >±0.3 ppm. [b] The resonance of these H4′ protons in the bis(tomaymycin)–d(CICGAATTCICG)$_2$ adduct overlap.

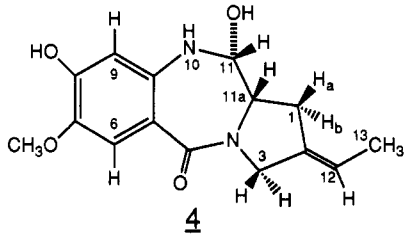

4

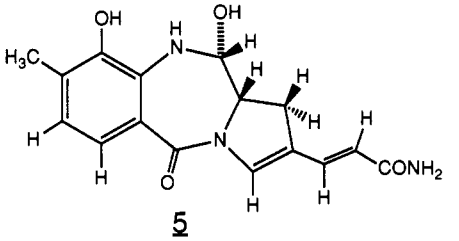

5

5′d(1C 2I 3C 4G 5A 6A 7T 8T 9C 10I 11C 12G)$_2$

6

FIGURE 2: Structures and numbering of tomaymycin (4), anthramycin (5), and the inosine-disubstituted d(CICGAATTCICG)$_2$ (6).

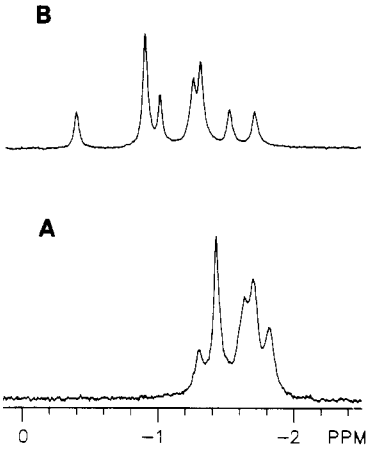

FIGURE 3: Proton-decoupled 202.44-MHz phosphorus NMR spectra of (A) the d(CICGAATTCICG)$_2$ duplex and (B) the tomaymycin–d(CICGAATTCICG)$_2$ adduct in buffered D_2O at 24 °C.

of the aforementioned aqueous (H_2O) buffer. This solution was heated at 60 °C for 5 min and then slowly allowed to cool to 4 °C overnight. This mixture was stirred at 4 °C for 4 days, at which time the resulting duplex adduct was separated from excess drug by conventional column chromatography. Chromatography was carried out at ambient temperature with hydroxylapatite as the adsorbent and a slow linear gradient of aqueous sodium phosphate buffer, pH 6.8, increasing from 10 to 200 mM and was monitored by absorbance at 254 nm. The appropriate duplex adduct fractions were adsorbed onto four Waters C-18 sep-paks connected in tandem. After the sep-paks were washed with water, the duplex adduct was eluted with 20% methanol in water, and the eluent was lyophilized to dryness.

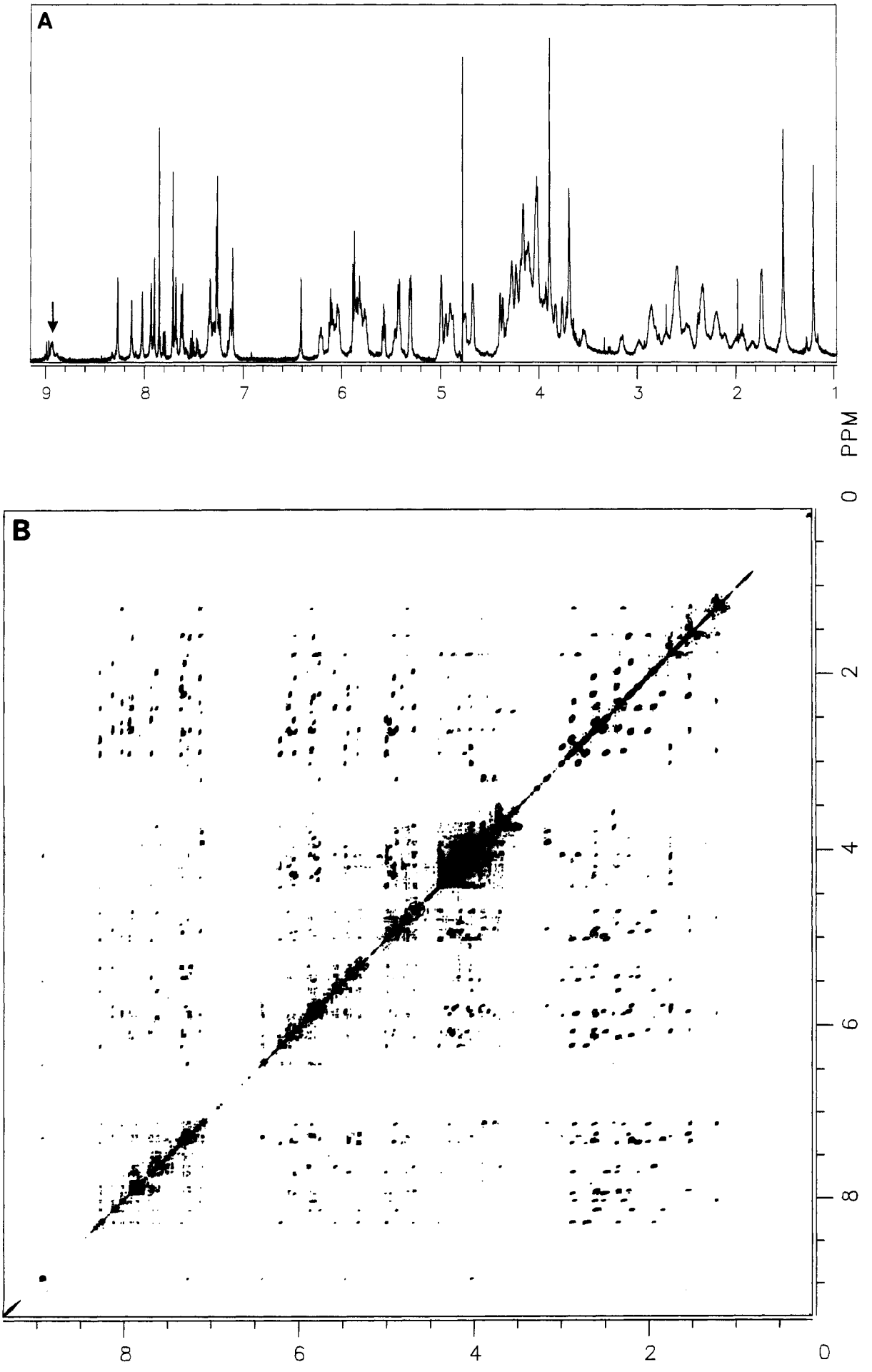
A
9
8
7
6
5
4
3
2
1
0 PPM
B
8
6
4
2
0

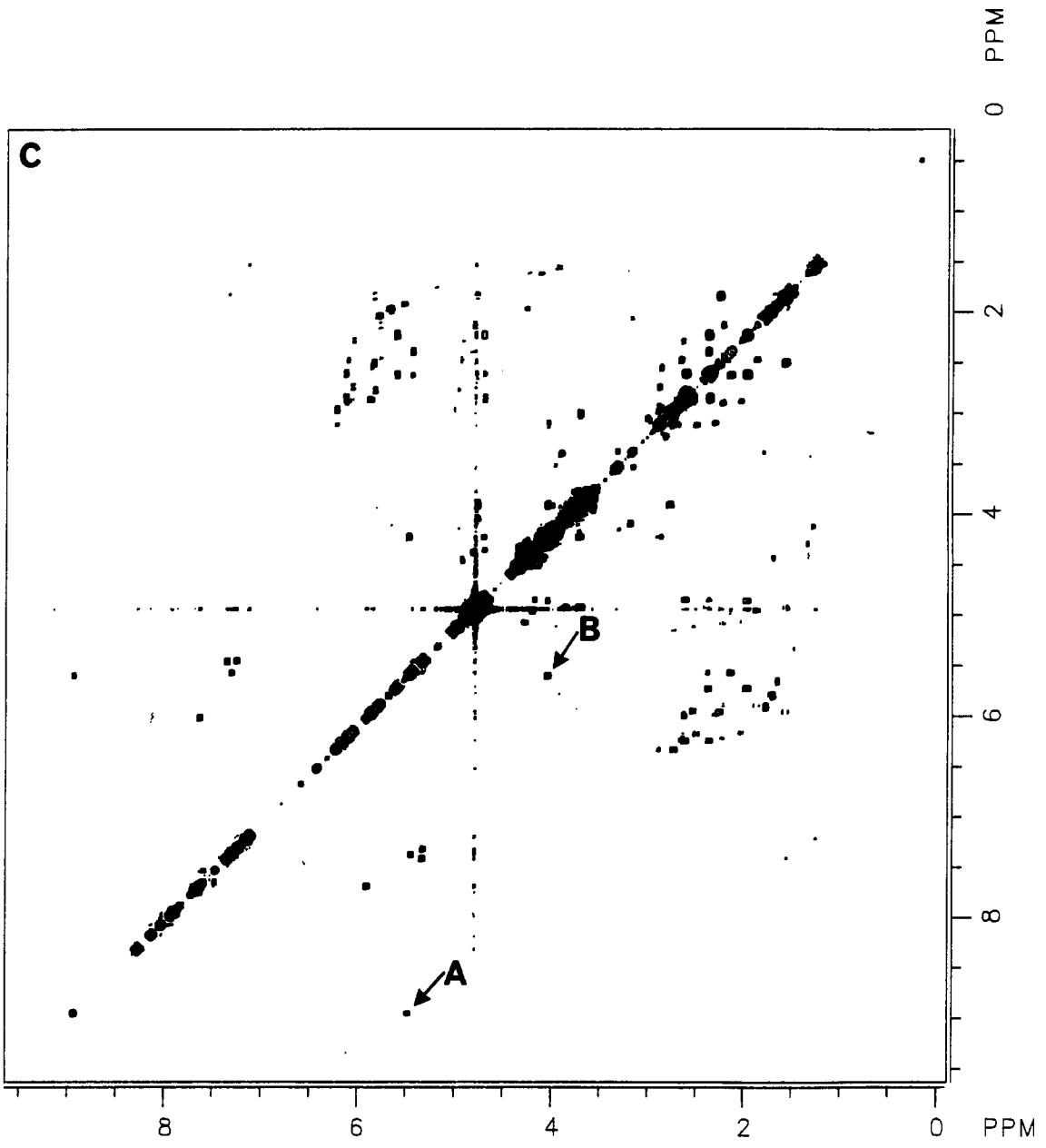

FIGURE 4: (A) 500-MHz proton NMR spectrum (0.9–9.2 ppm) of the bis(tomaymycin)-12-mer adduct in buffered D_2O at 24 °C. The arrow points to the nonexchanged ^{4}G amino proton. (B) Contour plot of the NOESY spectrum (250-ms mixing time) of the adduct at 24 °C. (C) Contour plot of the magnitude COSY spectrum at 24 °C. Arrow A shows the scalar coupling between the ^{4}G hydrogen-bonded amino proton and tomaymycin H11. Arrow B denotes the scalar coupling predicted for the 11*S* diastereomer of this adduct between the tomaymycin H11 and H11a protons.

(*B*) *Fluorescence Experiments.* The solution for fluorescence experiments was prepared by dissolving 17.7 A_{260} units of a lyophilized sample of the 12-mer adduct in 0.9 mL of water and diluting 3-fold with buffer. The final solution had A_{260} = 6.5 and A_{332} = 0.33 in a 1-cm cuvette. The tomaymycin concentration was 9.7×10^{-5} M, based on the absorbance at 332 nm and an extinction coefficient of 3.4×10^3 M^{-1} cm^{-1} for the tomaymycin–DNA adduct (Barkley et al., 1986). The dodecamer concentration was about 7.6×10^{-4} M duplex, based on the absorbance at 260 nm, an extinction coefficient of 7.4×10^3 M^{-1} cm^{-1} for the duplex, and an extinction coefficient of 9×10^3 M^{-1} cm^{-1} for tomaymycin (Arima et al., 1972). The extinction coefficient of the duplex was estimated from the base sequence (*CRC Handbook of Biochemistry and Molecular Biology*) with 20% hyperchromicity, assuming that guanosine and inosine mono- and dinucleotides have the same extinction coefficients. Unbound tomaymycin was removed by extraction 4 times with ethyl acetate and twice with ether. Ether was removed with a stream of N_2. The sample was placed in a 4 × 10 mm stoppered cuvette.

Proton NMR Experiments. NMR samples for the unmodified oligodeoxynucleotide and its bis(tomaymycin) adduct contained between 210 and 250 A_{260} units in 600 μL of 10 mM NaH_2PO_4, 100 mM NaCl, and 0.01 mM EDTA-buffered D_2O, pH 6.8. Samples were degassed with argon prior to NMR analysis. One- and two-dimensional proton and phosphorus NMR experiments in D_2O and H_2O were recorded on a GN 500 FT NMR spectrometer. Chemical shifts are reported in parts per million with positive values downfield from an external reference of 1 mg/mL TSP in D_2O for ^{1}H and an external reference of 85% H_3PO_4 in D_2O for ^{31}P resonances.

One-dimensional and NOE difference spectral analyses of

the nonexchangeable protons and exchangeable imino protons were performed on the D_2O sample and the same sample that had been lyophilized and redissolved in 90% H_2O/10% D_2O. Suppression of the H_2O signal was achieved with a 1–3–3–1 pulse sequence (Hore, 1983), and the exchangeable protons were assigned at 23, 15, 10, 5, and 0 °C as before (Graves et al., 1985). T_1 experiments were performed with the standard nonselective 180°–t_1–90° pulse sequence (Cheatham et al., 1988).

For all two-dimensional experiments a presaturation pulse was applied to suppress the HOD signal. Homonuclear scalar coupling was determined by using the standard-magnitude two-dimensional COSY and phase-sensitive two-dimensional double quantum filtered COSY. 2K complex points in t_2 and 256 points in the t_1 domain were acquired. Likewise, the phase-sensitive two-dimensional NOESY experiments were acquired with 2K data points in t_2 and 256 points in t_1. A pulse repetition time of 0.5 s was used for all COSY experiments and 2 s for each NOESY experiment. Mixing times of 50, 100, 250, and 400 ms were used for the phase-sensitive two-dimensional NOESY experiments and were stochastically varied to suppress cross peaks arising from scalar coupling (States et al., 1982). For all proton two-dimensional phase-sensitive experiments, a 45°-shifted sine bell function was applied to the data in both dimensions prior to transformation. For all two-dimensional proton experiments, the data were zero filled in t_1 such that the final frequency domain spectra consisted of 1K × 1K data matrices after symmetrization. Proton-decoupled phosphorus spectra were collected at 202.44 MHz. Phosphorus-detected, ^1H–^{31}P *J*-correlation experiments were performed according to the procedure described by Bax and Sarkar (1984).

Time-Resolved Fluorescence Studies. Fluorescence decay measurements were made by the time-correlated single-photon counting technique as described before (Barkley et al., 1986). Decay curves were acquired at 5 °C to about 15 × 10^3 counts in the peak. The data were fitted by reference deconvolution (Kolber & Barkley, 1986) to a sum of exponentials

$$i(\lambda_{ex},\lambda_{em};t) = \sum \alpha_i(\lambda_{ex},\lambda_{em}) \exp(-t/\tau_i)$$

with amplitudes α_i and lifetimes τ_i. In the case of ground-state heterogeneity, the amplitude α_i of component i depends on its molar extinction spectrum, fluorescence emission spectrum, radiative lifetime, and concentration. Decay curves measured at 313-, 337-, and 355-nm excitation wavelength and 420-nm emission wavelength were analyzed by a global program, assuming that the lifetimes but not the amplitudes are independent of wavelength (Knutson et al., 1983).

Molecular Modeling Studies. The crystal structure of TME (Arora, 1981) was used as the initial structure in this investigation. Partial atomic charges for tomaymycin with the methoxy group removed (for covalent bonding) were obtained from ab initio calculations as reported previously (Cheatham et al., 1988). The resulting structure was minimized by using the program AMBER 2.0 (Weiner & Kollman, 1984) and all atom force-field parameters (Weiner et al., 1984). A distance-dependent dielectric constant was used, and energy refinement was continued untl the rms gradient was less than 0.1 kcal/(mol Å). The cutoff distance for nonbonded pairs was 99 Å, and the nonbonded pair list was updated every 100 cycles. The heptanucleotide duplex structure d(CICG-AAT·GCICTTA) was constructed and brought to a minimum energy in the same way. The minimized tomaymycin structure was docked to this duplex near ^4G in four different orientations with the aid of the interactive graphics program MIDAS (Ferrin et al., 1988a,b). Each of the docked structures was brought to minimum energy as described above. Helix distortion energies were determined by subtracting the energy of the helix in the covalent complex from that of the separately minimized helix, and distortion induced in tomaymycin in the complex was determined in the same way.

Structural effects of water and counterions were neglected in energy calculations on the complexes. Although these effects influence the absolute values of binding energies, they should be negligible in comparisons of relative binding energies wherein the same drug is used at the same bonding site on the duplex.

Results

Proton NMR Comparison of the Inosine-Disubstituted Dodecamer [d(CICGAATTCICG)$_2$] with the Dickerson Dodecamer [d(CGCGAATTCGCG)$_2$]. The chemical shifts and T_1 relaxation times of select protons of the inosine-disubstituted 12-mer (Figure 2) are listed in Table I. Comparison of these results with previously published values (Reid, 1983) for the Dickerson dodecamer shows that the effect of substituting inosine for guanine at ^2G and ^{10}G on chemical shifts of oligodeoxynucleotide protons is minimal. Where changes occur, these are restricted to the base pairs containing the inosine and in rare instances to the adjacent base pair. For example, the imino protons of ^2I–^{11}C and ^3C–^{10}I move downfield by about 2 ppm, and the chemical shifts of nonexchangeable aromatic protons of ^2I and ^{10}I become more characteristic of adenine than guanine. In the deoxyribose moieties of ^2I and ^{10}I the H1′, H2′, and H2″ proton signals are shifted downfield relative to the equivalent guanines in the Dickerson dodecamer. For all other sugar protons observed, the chemical shift change is less than 0.05 ppm with the exception of ^9C and ^4G, where H1′ protons are shifted upfield by about 0.2 ppm.

The one-dimensional proton and two-dimensional COSY spectra of the inosine-disubstituted dodecamer are available (see paragraph at end of paper regarding supplementary material). The expected scalar cross peaks between the two thymine H6 and 5-CH_3 and four cytosine H5 and H6 protons are evident.

Symmetry of the Complex. (A) Phosphorus NMR Comparison of the d(CICGAATTCICG)$_2$ Duplex and Tomaymycin–d(CICGAATTCICG)$_2$ Adduct. A comparison of the proton-decoupled phosphorus spectra of d(CICGAATTCICG)$_2$ and its tomaymycin adduct is shown in parts A and B of Figure 3, respectively. While the individual phosphorus chemical shifts have changed in the 12-mer adduct species relative to the duplex alone, the overall complexity (i.e., the number of ^{31}P resonance signals) of the spectrum has not changed appreciably. In each case approximately 11 phosphorus resonances can be identified (see later in Figure 9). The constant number of phosphorus resonances in the duplex and its 12-mer adduct implies that the duplex adduct has maintained the self-complementarity of the duplex and therefore has become associated with an *even* number of tomaymycin molecules (presumably two), each of which is *equivalent* in all respects. One of the phosphorus signals in the 12-mer adduct has shifted downfield, most likely indicative of a structural perturbation of the deoxyribose phosphate backbone as a consequence of tomaymycin bonding to the 12-mer duplex (see later).

(B) Nonexchangeable Proton Assignments in the Tomaymycin–d(CICGAATTCICG)$_2$ Adduct. The 500-MHz proton NMR of the tomaymycin–d(CICGAATTCICG)$_2$ adduct is shown in Figure 4A. The majority of the signals are well resolved and have been assigned by two-dimensional NMR

Table II: Comparison of the Nonexchangeable Proton Chemical Shift[a] Assignments (ppm) in Tomaymycin[b] Alone and in the Tomaymycin–12-mer Duplex Adduct

species	H1's[c]	H3's[c]	H6	7-OCH$_3$	H9	H11	H11a	H12	H13
tomaymycin (11*R*,11a*S*)	2.97, 2.69	4.25, ~4.28	7.28	3.28	6.22	4.58	3.96	5.44	1.66
tomaymycin–12-mer duplex adduct	2.97, 2.78	3.15, 3.90	7.10	3.88	6.40	5.48	3.99	5.75	1.70
$\Delta\delta$	*c*	*c*	−0.18	+0.66[d]	+0.18	+0.90	+0.03	+0.31	+0.04

[a] Chemical shifts are in parts per million using TSP as an internal reference. [b] For numbering of tomaymycin, see Figure 2. [c] Individual chemical shift assignments for each pair of H1 and H3 protons were not made, and therefore $\Delta\delta$ values are omitted. [d] Underlined are $>\pm 0.3$ ppm.

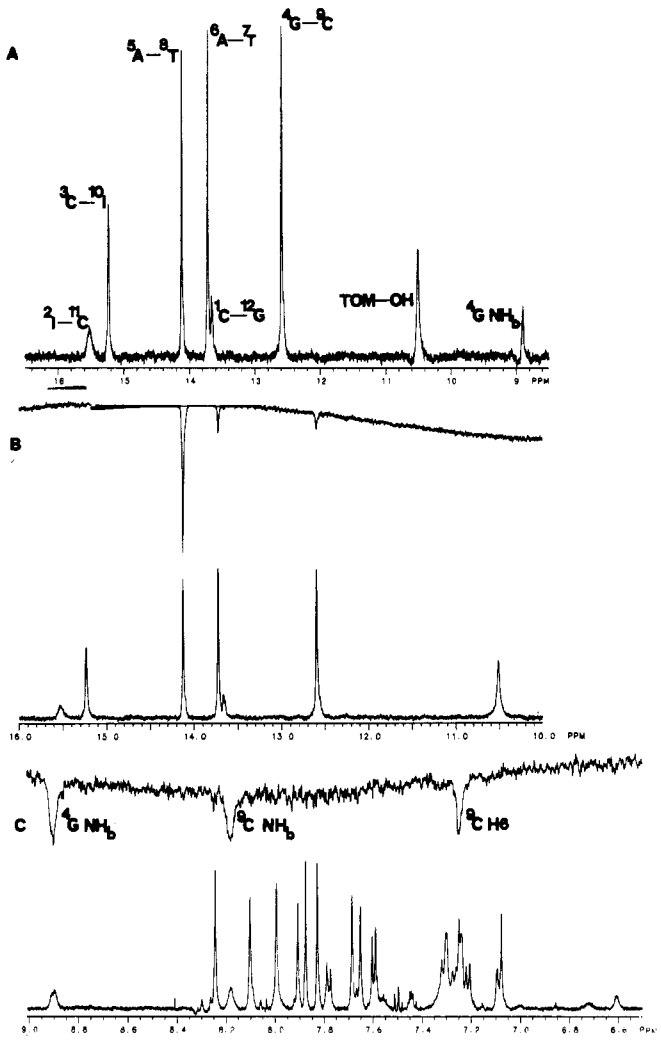

FIGURE 5: (A) 500-MHz proton NMR spectrum (12–16 ppm) of the bis(tomaymycin)–d(CICGAATTCICG)$_2$ adduct in buffered 90% H_2O/10% D_2O, pH 6.8 at 24 °C. One-dimensional NOE difference spectra following saturation (2 s) of (B) the 14.13 ppm and (C) the 12.59 ppm exchangeable resonances in the complex. The assignments of the imino protons of the complex and the phenolic proton of tomaymycin at 10 °C are listed in Tables I and II.

spectra utilizing through-bond (COSY) and through-space (NOESY) connectivities (see later). The phase-sensitive NOESY (mixing time 250 ms) and magnitude COSY spectra are plotted in parts B and C of Figure 4, respectively. The chemical shift assignments for the nucleotide and tomaymycin protons in the duplex and the tomaymycin–duplex adduct are listed in Tables I and II.

A comparison of the proton spectra of the duplex and tomaymycin–duplex adduct does not reveal any increase in complexity; i.e., same number of resonances are found in both spectra, except for an additional set of tomaymycin proton resonances in the duplex adduct. This observation confirms the symmetry of the tomaymycin–duplex adduct revealed also in the phosphorus spectra (Figure 3).

Identification of the Covalent Linkage Sites between Tomaymycin and DNA in the Bis(tomaymycin)–d(CICGAATTCICG)$_2$ Adduct. The proton NMR of the imino region of the bis(tomaymycin)–d(CICGAATTCICG)$_2$ adduct in 90% H_2O is plotted in Figure 5A. Six imino proton signals are found in the region between 12 and 16 ppm and are identified in Table I. These were assigned by one-dimensional NOE experiments, and a representative NOE difference spectrum is shown in Figure 5B. The two protons upfield of the imino region in Figure 5A are the tomaymycin phenolic proton (10.5 ppm) and the ^{4}G hydrogen-bonded 2-amino proton (8.95 ppm). The assignment of the ^{4}G hydrogen-bonded 2-amino proton (NH_b) was made by irradiation of the ^{4}G imino proton and observation of the nonexchangeable base and amino proton region (7.0–9.0 ppm) (Figure 5C). Irradiation of the ^{4}G–^{9}C imino proton results in NOEs into the ^{4}G NH_b, ^{9}C NH_b, and most likely the ^{9}C H6.

The ^{4}G NH_b proton identified through the one-dimensional NOE experiment (see Figure 5C) also appears in the one-dimensional proton spectrum run in D_2O (arrow in Figure 4A). Normally guanine amino protons in duplex DNA are rapidly exchanged in D_2O, but in this case the exchange is relatively slow, suggesting tomaymycin modification of the duplex at this site.[3] In the magnitude COSY (Figure 4C) scalar coupling is evident between ^{4}G NH_b and the proton at C-11 of tomaymycin (arrow A). This establishes the points of covalent attachment between tomaymycin and d(CICGAATTCICG)$_2$ as C-11 and the ^{4}G exocyclic 2-amino nitrogen, respectively.

Determination of the Covalent Linkage Site Geometry and Orientation of Tomaymycin in the Minor Groove of d(CICGAATTCICG)$_2$. (A) Molecular Modeling Predictions. In principle, tomaymycin can assume four different binding modes while covalently bonded through N2 of ^{4}G on d(CICGAATTCICG)$_2$. Thus four different binding modes were modeled: the *R* and *S* configurations at C-11 of tomaymycin, each with the drug positioned in the minor groove so that its aromatic ring was pointing toward the 3′ end or the 5′ end of the covalently bound strand of d(CICGAATGCICTTA). Following energy minimization in AMBER, the net binding energy for each species was calculated from its total intermolecular drug–DNA binding energy minus the helix and drug distortion energies that resulted from the induced fit (Table III). There was a preference by 2.9 kcal/mol for the covalent adduct with 11*S* configuration and the benzene ring toward the 3′ direction over the 5′-oriented adduct with the same stereochemistry. While the molecular mechanics results clearly rule out both 11*R* diastereomers, the difference of 2.9 kcal/mol is considered insufficient to definitely differentiate between the two 11*S* diastereomers.

The explanation for the greater stability of the pair of 11*S* diastereomers lies not in differences in distortion energies but

[3] It is pertinent to note that Gao and Patel (1989) have observed separate resonance signals for the guanine 2-amino hydrogen-bonded (NH_b) and exposed protons (NH_e) in the chromomycin–DNA complex at around 8.1–8.6 and 5.7–6.7 ppm, respectively. Presumably, the bound chromomycin molecule prevents the N2 guanine protons from rapidly exchanging, as normally occurs in duplex molecules.

Table III: Energies (kcal/mol) of Covalent Complexes between Tomaymycin and d(CICGAAT·GCICTTA)[a]

			intermolecular			distortion[c]			
config at C-11	direction[b]	total	steric	elstat	total	drug	DNA	total	net binding[d]
S	3′	−443.5	−25.7	−13.4	−39.1	0.1	17.8	17.9	−21.2
S	5′	−440.6	−29.2	−9.9	−39.1	1.0	19.7	20.7	−18.3
R	3′	−420.9	−15.0	−8.4	−23.4	2.5	22.2	19.7	−3.7
R	5′	−432.3	−24.6	−7.0	−31.6	2.3	19.3	21.6	−10.0

[a] These energies are valid only for comparison within the table. They should not be compared with other drugs or other DNA segments. [b] Direction refers to orientation in the minor groove. 3′ and 5′ are oriented with the aromatic ing to 3′ or 5′ sides, respectively. [c] Drug distortion and helix distortion energies equal their values in the complex less their values when minimized alone (18.8 and −441.1 kcal/mol, respectively). [d] Net binding energy equals the total intermolecular binding minus the total distortion energy.

Table IV: Energies (kcal/mol) for the Interactions of Tomaymycin with Individual Residues of d(CICGAAT·GCICTTA)[a]

species		residue					
config at C-11	direction	^{4}G	^{5}A	^{11}C	11,12P	12P 12,13P	^{13}S[b]
S	3′	−3.6	−4.7		−4.0		
S	5′	−3.1				−4.5	−4.7
R	3′	−3.1		−3.0			
R	5′	−3.9				−3.4	

[a] Only energies >−3.0 kcal/mol are listed. [b] S stands for sugar.

Table V: Fluorescence Decay Data for Tomaymycin Bound to Calf Thymus DNA, $d(ATGCAT)_2$, and $d(CIGCAATTCICG)_2$[a]

	λ_{ex} (nm)	α_1[b]	τ_1 (ns)	α_2	τ_2 (ns)
calf thymus DNA[c]	313	0.35	3.8	0.65	6.7
	337	0.31		0.69	
	355	0.28		0.72	
$d(ATGCAT)_2$	313	0.43	2.3	0.57	5.7
	337	0.52		0.48	
	355	0.63		0.37	
$d(CIGCAATTCICG)_2$	313	0.11	1.6	0.89	6.4
	337	0.08		0.92	
	355	0.08		0.92	

[a] Decay parameters were obtained by global analysis of decay curves measured at the indicated excitation wavelengths and emission wavelengths between 390 and 490 nm. [b] Fractional amplitudes $\sum\alpha_i = 1$. [c] Data for pH 7.5, 5 °C, from M. D. Barkley, F. N. Chowdhury and K. Maskos (manuscript in preparation). Amplitudes and lifetimes are independent of pH in the range 6.4–9.0.

in intermolecular binding energies (Table IV). Through a combination of steric and electrostatic interactions, where steric binding energies predominate, the 11*S* diastereomers are favored equally over 11*R* diastereomers. According to these calculations the 3′ orientation is then marginally favored over the 5′ orientation on the basis of the relative distortion energies required for bonding in tomaymycin and DNA.

(*B*) *Fluorescence Studies.* Previously we showed that there are two fluorescent ground-state forms of tomaymycin in protic solvents and on calf thymus DNA and $d(ATGCAT)_2$ (Barkley et al., 1986; Cheatham et al., 1988). We argued that the longer lifetime component represents the 11*S*,11a*S* diastereomeric adduct, while the shorter lifetime component represents the 11*R* adduct. In contrast, we found essentially one fluorescent species of tomaymycin on $d(CICGAATTCICG)_2$, corresponding to the longer lifetime component or the 11*S*,11a*S* diastereomer (Table V). The fluorescence decay of the tomaymycin–$d(CICGAATTCICG)_2$ adduct gave an acceptable fit to a monoexponential function with a $\chi_r 2$ value of 1.4 and a lifetime of 6.4 ns. A slightly better fit with $\chi_r 2$ = 1.2 was obtained by assuming a biexponential function. Including the second exponential term in the data analysis had little effect on the lifetime of the predominant species. As seen in Table V, the 6.4-ns lifetime lies within the range of values associated with the 11*S* diastereomeric adduct in calf thymus DNA and $d(ATGCAT)_2$. On the basis of the relative decay amplitudes α_i in the bis(tomaymycin)–$d(CICGAATTCICG)_2$ adduct, the 11*S* diastereomer is present in at least 10-fold excess over the short-lifetime species. The 1.6-ns lifetime may be due to small amounts of unbound tomaymycin, a second species of the tomaymycin–duplex adduct, or an unresolved mixture of the two. Molecular modeling data (Table III) would suggest that the second most energetically favored species is the 11*S*, 5′-oriented adduct. Since this species should have the longer lifetime (6.4 ns), we propose that the small amount of the second species observed by fluorescence is free tomaymycin. Attempts to fit the fluorescence decay to a triexponential function were unsuccessful.

(*C*) *Proton NMR Studies.* (*1*) *Stereochemistry at the Covalent Linkage Site.* Examination of the magnitude COSY spectrum of the bis(tomaymycin)–$d(CICGAATTCICG)_2$ adduct shows scalar coupling of the 11 and 11a protons of tomaymycin (arrow B in Figure 4C). In addition to firmly assigning the 5.48 ppm resonance signal to the proton at C11 of tomaymycin (which is shifted downfield by 0.9 ppm relative to its chemical shift in free tomaymycin), the scalar coupling of protons at C11 and C11a potentially provides stereochemical information on the linkage site geometry.[4] In TME only the 11*S*,11a*S* diastereomeric species shows scalar coupling between protons at C11 and C11a because the dihedral angle between these protons in the 11*R*,11a*S* diastereomer is close to 90° (Barkley et al., 1986). Molecular modeling using AMBER was carried out on both diastereomeric species (11*R*,11a*S* and 11*S*,11a*S*) of tomaymycin bound covalently to the inosine-disubstituted dodecamer with each having a 3′ orientation of the aromatic ring of tomaymycin to ^{4}G. Only these two species were modeled since the NOE data narrowed down the four possible species to the 3′-oriented adducts (see later). The results showed that *only* the 11*S*,11a*S* species was predicted to have significant scaler coupling between protons at C11 and C11a; i.e., the dihedral angles between the protons at C11 and C11a in the 11*S* and 11*R* species are predicted to be 175.7° and 71.5°, respectively. The assignment of the species of tomaymycin bound to 12-mer duplex as the 11*S*,11a*S* diastereomer is also consistent with the fluorescence results (see Table V).

(*2*) *Orientation of Tomaymycin in the Minor Groove of the 12-mer Duplex.* In principle, the tomaymycin molecule may be oriented with the aromatic ring either to the 3′ side or to the 5′ side of covalently modified guanine in the 12-mer adduct. To assign the orientation of tomaymycin in the minor

[4] In a previous paper on tomaymycin–$d(ATGCAT)_2$ (Cheatham et al., 1988), we had only reported one set of scalar cross peaks for coupling of the 11 and 11a protons. However, there is a second set of scalar cross peaks for the 11 and 11a protons that we had overlooked. For this second set, reported for the first time, the proton at C-11 has a chemical shift of 4.42 ppm. Molecular modeling using AMBER (Remers, unpublished results) predicts scalar coupling between the protons at C11 and C11a for *both* tentatively identified tomaymycin–$(ATGCAT)_2$ adducts (11*S*, 3′ orientation, and 11*R*, 5′ orientation), in contrast to the results reported here for the equivalent bis(tomaymycin)–12-mer adducts.

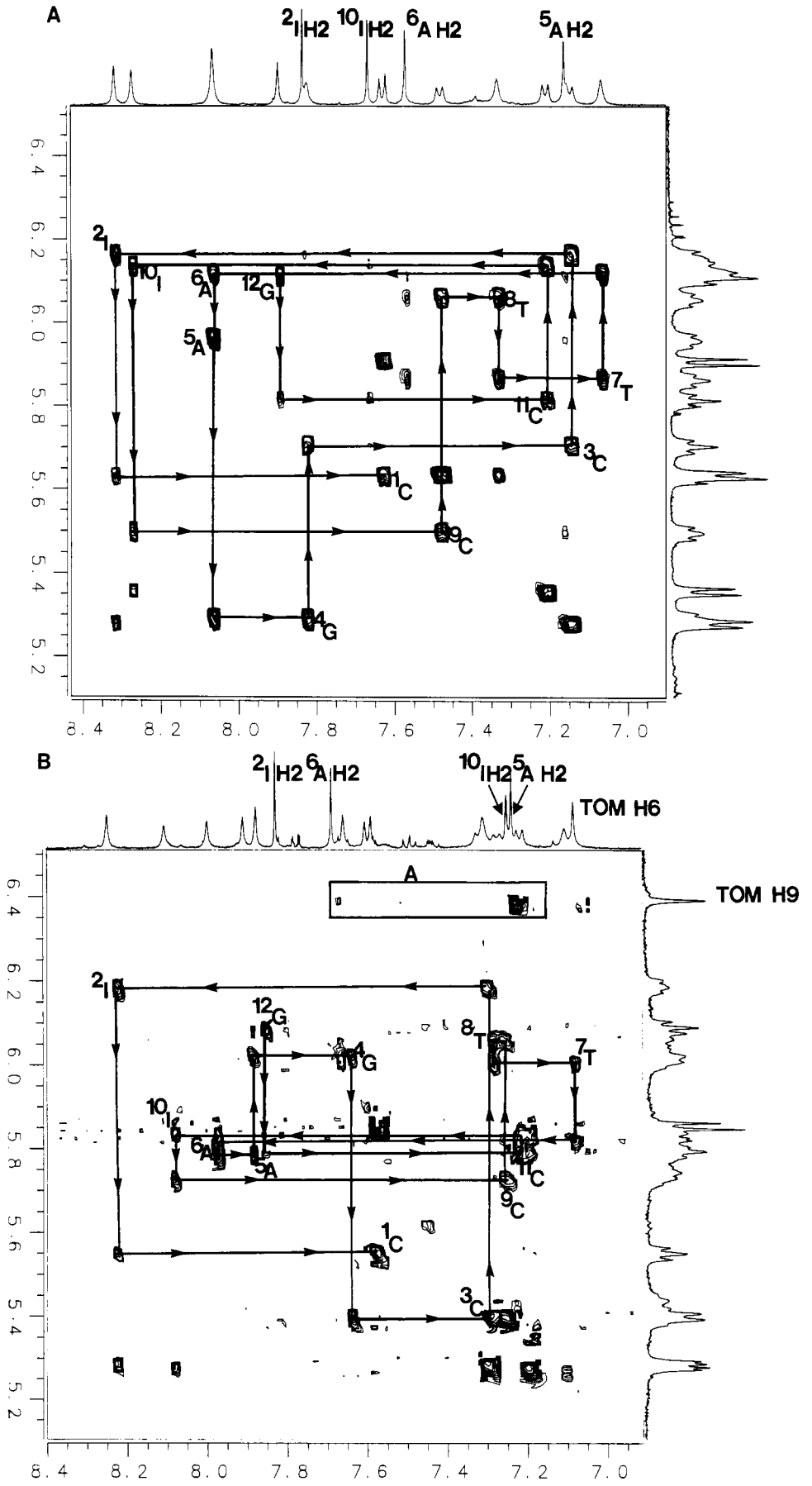

FIGURE 6: Phase-sensitive NOESY (250-ms mixing time) expanded contour plots of the Pu H8 and the Py H6 to H1′ protons for the (A) duplex and (B) duplex adduct. Intranucleotide cross peaks are indicated and the sequential 3′ to 5′ walks between the base and H1′ protons are traced. Box A in panel B shows the tomaymycin H9 cross peaks to ^{5}A and ^{6}A H2s.

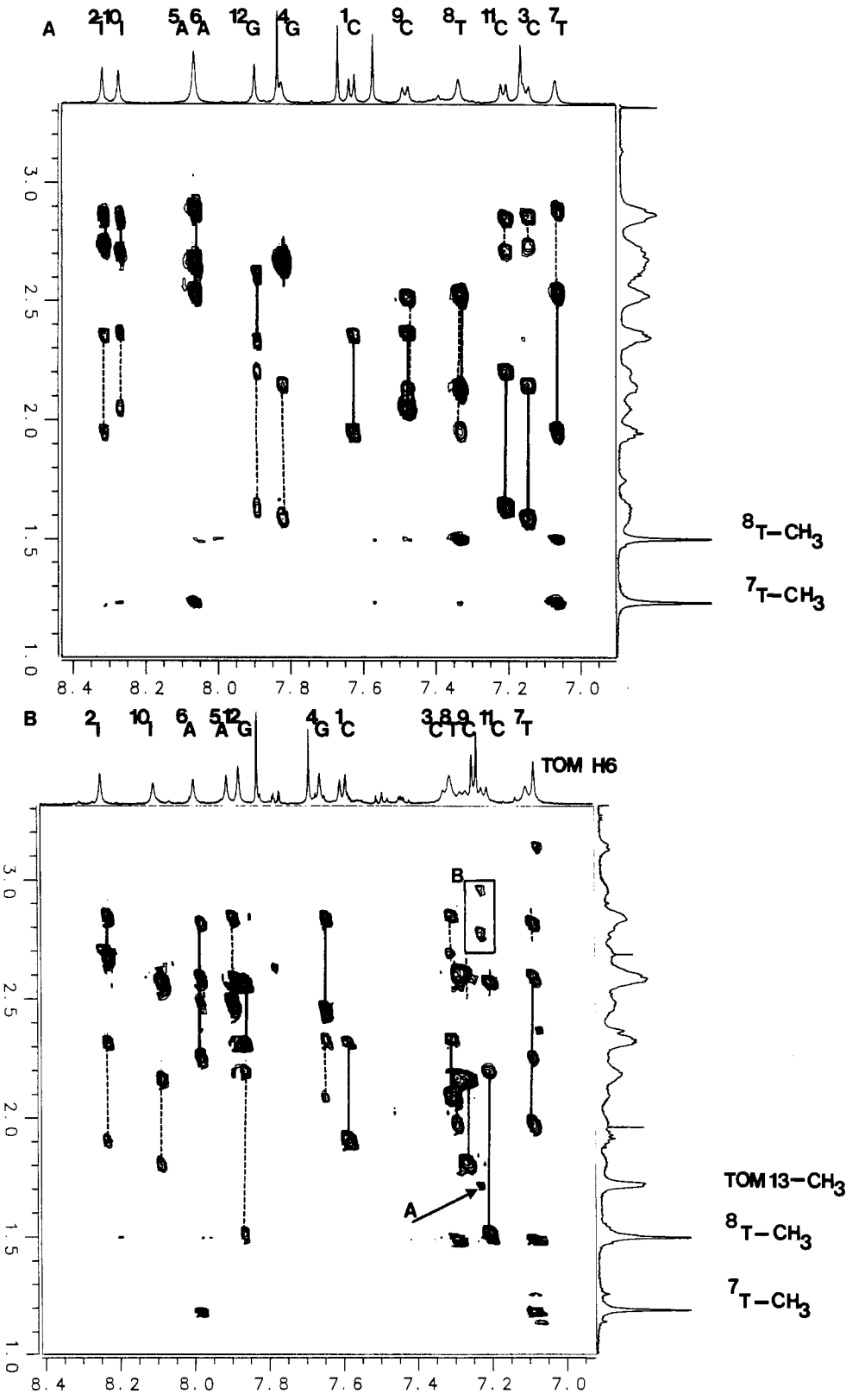

FIGURE 7: Phase-sensitive NOESY (250-ms mixing time) expanded contour plots of the Pu H8 and Py H6 to H2′ and H2″ protons for the (A) duplex and (B) duplex adduct. Intranucleotide connectivities are indicated with solid lines. Internucleotide connectivities are indicated with broken lines. Arrow A and box B in panel B denote the cross peak(s) between ^{10}I H2 and the tomaymycin ethylidene methyl (A) and H1a and H1b (B), respectively.

groove of DNA, specific intermolecular drug–nucleotide NOEs need to be identified between unambiguously assigned tomaymycin and deoxynucleotide protons. Molecular modeling studies show that the H9 and ethylidene methyl protons of tomaymycin are in proximity to the floor of the minor groove of DNA (Petrusek et al., 1982). Adenine and inosine H2s that are located in the minor groove are potential "reporter atoms" to detect tomaymycin protons via NOE cross peaks. In the expanded NOESY spectrum (Figure 6B) cross peaks are evident between the tomaymycin H9 and both ^{5}A and ^{6}A H2 protons (box A). In addition, a NOE cross peak is found between the tomaymycin ethylidine methyl and a ^{10}I H2 proton

Table VI: Tomaymycin–Nucleotide Interproton Distances Determined in the Energy-Minimized Species Having 11*S* Stereochemistry with either a 3′ or 5′ Orientation

species	protons[a] T[b]		12-mer	distance (Å)
11*S*, 3′	13-CH_3	to	^{10}I H2	3.59[c]
	H9	to	^{5}A H2	2.96
	H9	to	^{6}A H2	6.03
	H1a	to	^{10}I H2	2.28
	H1b	to	^{10}I H2	2.64
11*S*, 5′	13-CH_3	to	^{5}A H2	3.82[c]
	H9	to	^{10}I H2	2.53

[a] For tomaymycin numbering, see Figure 2. [b] Tomaymycin. [c] Average for all three C–H bonds.

(Figure 7B, arrow A). Confirmation of these NOEs was obtained by one-dimensional NOE difference experiments, and the critical assignments of adenine and inosine H2 protons were made by one-dimensional NOE difference experiments from imino protons (unpublished experiments).

(D) Molecular Modeling Studies on the 3′- and 5′-Oriented 11S Adducts. Since the stereochemistry at the covalent linkage site had been unambiguously assigned by both fluorescence and proton NMR, just the 3′ and 5′ orientations were modeled with AMBER (Table VI). Of the two species modeled, only the tomaymycin adduct having the 3′ orientation gave nucleotide–drug interproton distances that were in accord with the one- and two-dimensional NOE experiments (Figures 6B and 7B). For example, this species (3′ orientation, 11*S* stereochemistry) is predicted to have drug–nucleotide intermolecular distances <4.0 Å for the tomaymycin 13-CH_3 to ^{10}I H2, tomaymycin H9 to ^{5}A H2, and tomaymycin H1a and H1b to ^{10}I H2. NOE cross peaks are evident for all four of these sets of protons (Figures 6B and 7B). In contrast, NOE cross peaks that are predicted for the 5′-oriented, 11*S* species in the NOESY spectrum (i.e., tomaymycin 13-CH_3 to ^{5}A H2 and tomaymycin H9 to ^{10}I H2) are absent.

(E) Conclusions from Combined Fluorescence, NMR, and Molecular Modeling Studies. The fluorescence and COSY data provide independent evidence for the 11*S* stereochemistry at the covalent linkage site. One- and two-dimensional NOE data provide the necessary interproton drug–nucleotide cross peaks to assign the 3′ orientation of tomaymycin in the 12-mer duplex adduct. Therefore the species of tomaymycin bound to ^{4}G in the 12-mer duplex adduct has an 11*S* stereochemical linkage to N2 of guanine, and the aromatic ring of tomaymycin lies to the 3′ side of ^{4}G.

Assignments of Deoxynucleotide Proton and Phosphorus Resonances in the 12-mer Adduct and Effect of Tomaymycin Bonding on Backbone and Sugar Geometry of d(CICGAATTCICG)$_2$. (A) Two-Dimensional NOESY Experiments. Parts A and B of Figure 6 show expanded contour plots of the phase-sensitive NOESY (250 ms) for the base and H1′ protons of d(CICGAATTCICG)$_2$ in both the 12-mer duplex and bis(tomaymycin)–12-mer adduct. The one-dimensional spectra are drawn above the plots to illustrate the ample resolution between the individual nucleotide resonances, which simplified the task of resonance assignments. As observed in these figures, purine H8 and pyrimidine H6 protons exhibit NOEs to their own H1′ protons and to the H1′s of their 5′ neighbors, charateristic of a right-handed duplex (Hare et al., 1983; Reid, 1987; Patel et al., 1987). With these connectivities established, assignments of the majority of the oligodeoxynucleotide sugar protons (except H5′s) can likewise be made by using NOE cross peaks between the base and other sugar protons (Table 1B). These assignments are further confirmed with the complementary scalar coupling observed in the two-dimensional COSY spectrum.

The assignments of sugar H2″ and H2′ protons in the 12-mer and bis(tomaymycin)–12-mer adduct are made from their NOESY cross peaks to inter- and intranucleotide base protons (Figure 7). In addition, qualitative analysis of the base H8/H6 to H2″ and H2′ proton NOESY cross peaks at lower mixing times (50 and 100 ms) is a recognized means to evaluate the purine $O_{1'}$–$C_{1'}$–N_9–C_4 and pyrimidine $O_{1'}$–$C_{1'}$–N_1–C_2 glycosidic dihedral angle ranges syn, anti, and high anti (Hosur et al., 1986; Kumar et al., 1985; Chary et al., 1987). From the data in Tables VII and VIII we tentatively conclude that a significant number of glycosidic dihedral angles in the unmodified duplex are in the high-anti domain (^{2}I, ^{7}T, ^{8}T, ^{10}I, ^{12}G), which suggests a DNA structure deviant from the classical B-form.[5] Two of the high-anti glycosidic angles are associated with substitution of deoxyinosine for deoxyguanosine into the dodecamer (^{2}I, ^{10}I). The high-anti glycosidic dihedral angle for nucleotide ^{12}G may be due to fraying at the oligomer termini, because this linkage is not as restricted as those more internal. In the bis(tomaymycin)–d(CICGAATTCICG)$_2$ adduct, only nucleotide ^{8}T continues to exhibit a glycosidic dihedral angle in the high-anti form, with the remainder of the nucleotides having glycosidic dihedral angles in the anti range, which is consistent with a B-form DNA.

The nonscalar cross peaks between base H8/H6 and sugar H2″ and H2′ protons have also been used to distinguish between A- and B-type helices (Haasnoot et al., 1984). In the case of A-type DNA, the C3′-endo sugar geometry predominates and internucleotide cross peaks between H8/H6 protons to the 5′-neighboring H2′ protons are stronger than those to the corresponding intranucleotide H2′ protons. The converse is true for B-type DNA, where C2′-endo sugar geometry predominates and the intranucleotide distances are shorter. The intensities of these cross peaks at lower mixing times (50 and 100 ms) were used to *qualitatively confirm* the sugar geometry assignments made from the scalar coupling observed or absent in the two-dimensional COSY (see below).

(B) Two-Dimensional COSY Experiments. Since the vicinal coupling constants of DNA sugar ring protons vary as a function of pseudorotation angle or sugar pucker, it is possible to assign sugar geometries to each nucleotide on the basis of observed or absent scalar cross peaks between the sugar protons listed in Table IB. As an example, one strong indicator of difference in sugar geometry is the comparison of cross-peak intensity between protons of H1′ and H2″ and H1′ and H2′, as shown for the bis(tomaymycin)–d(CICGAATTCICG)$_2$ adduct (Figure 8). In the case of C2′-endo geometry for classical B-type DNA helices, strong scalar cross peaks between protons of H1′ and H2″ and H1′ and H2′ are expected. Conversely for C3′-endo geometries, or A-type DNA helices, the *J* couplings of H1′ to H2′ are expected to be weak or absent. With this concept, the results show that, for most nucleotides in the 12-mer and the 12-mer adduct, the sugar geometries are mostly around or near C2′-endo or near O1′-endo (Tables VII and VIII). In the duplex ^{3}C, ^{7}T, and ^{11}C are exceptions, where the average C3′-endo sugar geometry of A-form helices predominates. Upon adduct formation of this duplex with tomaymycin, only at ^{11}C is the C3′-endo geometry still present. For nucleotides ^{3}C and ^{7}T, there is a

[5] We are hesitant to place too much emphasis on the conclusions listed in Tables VII and VIII. As a referee correctly pointed out, our conclusions are based upon qualitative trends in NOESY and COSY data sets. Until quantitative information is available, these should only be considered tentative.

Table VII: Structural Information from the Relative Intensities[a] of COSY[b] and NOESY[c] Cross Peaks for d(CIGCAATTCICG)$_2$

	NOESY, NOE from H8/H6 to		inference, glycosidic	COSY, J coupling					
				H1′ with		H3′ with			inference,
base	H2″	H2′	angle	H2″	H2′	H2″	H2′	H3′ with H4′	sugar pucker
^{1}C	W	S	anti	S	S	W	S	S	O1′-endo
^{2}I	S	S	high anti	O (W)	M	A	O (M)	M	C1′-exo
^{3}C	W	S	anti	S	W	W	O (M)	O (S)	C3′-endo
^{4}G	O	O		S	S	A	W	W	C3′-exo
^{5}A	O	O		M	M	A	O (M)	S	O1′-endo
^{6}A	O	O		O (W)	O (M)	A	M	O (S)	O1′-endo
^{7}T	S	S	high anti	M	W	A	M	S	C3′-endo
^{8}T	S	S	high anti	M	W	A	M	S	O1′-endo
^{9}C	M	S	anti	S	M	A	M	S	O1′-endo
^{10}I	S	S	high anti	O (M)	O (M)	A	O (M)	O (S)	O1′-endo
^{11}C	W	S	anti	S	W	A	O (M)	S	C3′-endo
^{12}G	S	M	high anti	O (M)	S	S	W	S	O1′-endo

[a] A = absent; W = weak; M = moderate; S = strong; O = overlapping. Partially resolved cross-peak intensities are placed in parentheses. [b] Magnitude COSY and two-dimensional phase-sensitive double quantum filtered COSY cross peaks are examined. See Materials and Methods for details. [c] Data from phase-sensitive two-dimensional NOESY experiments with mixing times of 50 and 100 ms. See Materials and Methods for details.

Table VIII: Structural Information from the Relative Intensities[a] of COSY[b] and NOESY[c] Cross Peaks for the Bis(tomaymycin)–d(CICGAATTCICG)$_2$ Adduct

	NOESY, NOE from H8/H6 to		inference, glycosidic	COSY, J coupling					
				H1′ with		H3′ with			
base	H2″	H2′	angle	H2″	H2′	H2″	H2′	H3′ with H4′	inference, sugar pucker
^{1}C	A	S	anti	S	S	A	S	S	O1′-endo
^{2}I	W	S	anti	M	S	A	W	W	C1′-exo–C2′-endo
^{3}C	W	S	anti	M	S	M	W	O (S)	C1′-exo
^{4}G	W	S	anti	W	M	A	A	A	C1′-exo–C2′-endo
^{5}A	(W)	O (S)	anti	W	M	A	W	O (W)	C1′-exo–O1′-endo
^{6}A	W	S	anti	W	M	A	A	O (M)	C1′-exo–O1′-endo
^{7}T	W	S	anti	M	M	A	W	O (W)	C1′-exo–O1′-endo
^{8}T	S	S	high anti	O (M)	M	A	W	O (W)	C1′-exo–O1′-endo
^{9}C	(W)	M	anti	M	A	W	O (M)	O (W)	O1′-endo
^{10}I	O	O		O	O	A		O	
^{11}C	W	S	anti	O (S)	M	A	O	O (S)	C3′-endo
^{12}G	(S)	M	anti	O (S)	S	S	S	S	O1′-endo

[a–c] For footnotes, see Table VII.

shift toward more B-like structure upon adduct formation.

(*C*) *Two-Dimensional Proton–Phosphorus J-Correlation Experiments.* The majority of the phosphorus resonances in d(CICGAATTCICG)$_2$ only undergo small changes in chemical shift upon covalent modification with tomaymycin. However, one phosphorus resonance is significantly shifted downfield from the others (compare parts A and B of Figure 3). This result is reminiscent of previous work in our laboratory with covalent bonding of anthramycin to d(ATGCAT)$_2$ (Boyd et al., 1990). This observed downfield shift of the phosphorus resonance suggests a structural perturbation of the phosphate backbone as a result of covalent bonding. The contour plot of the phase-sensitive two-dimensional heteronuclear phosphorus-detected ^{31}P–^{1}H J-correlation experiment is shown in Figure 9. Cross peaks connect the downfield-shifted phosphorus resonance to the ^{3}C H3′ and ^{4}G H4′, indicating that the perturbation of the phosphate backbone is localized to the 5′ side of the drug covalent bonding site.

Molecular Modeling of the Duplex and the Tomaymycin–Duplex Adduct. A 7-mer duplex [d(CICGAAT·ATTCICG)] containing a single tomaymycin bonding site (^{4}G) and its 11*S*, 3′-oriented tomaymycin–duplex adduct were energy minimized by using AMBER. Of the 14 sugars in the 7-mer duplex, nine were calculated to be C2′-endo, two O1′-endo, and three C1′-exo. Exactly the same pattern was found for the 11*S*, 3′-oriented tomaymycin–duplex adduct, except that it has a C1′-exo pucker for the ^{2}I sugar rather than a C2′-endo pucker. No significant differences were found in backbone dihedrals or torsional angles (χ) involving base–sugar linkages. The energy for the base pair ^{4}G–^{11}C is −15.3 kcal/mol in the tomaymycin–duplex adduct, compared with −21.6 kcal/mol for the 7-mer duplex. This magnitude of decrease was found for the base pair where a covalent bond to N2 of guanine occurs in anthramycin–d(ATGCAT)$_2$ (Boyd et al., 1990). No other significant differences were found for base-stacking energies.

Discussion

Structure of the Bis(tomaymycin)–12-mer Adduct. It has long been assumed on the basis of indirect evidence that the P(1,4)Bs covalently bond via C-11 to the exocyclic 2-amino group of guanine on DNA as shown in Figure 1 (Kohn et al., 1974; Hurley & Petrusek, 1979). However, it is only now through the results described in this paper that this has been unequivocally demonstrated. The proton NMR assignment of the ^{4}G hydrogen-bonded amino proton (Figure 5C) was crucial for this conclusion. Because of the covalent linkage of the ^{4}G amino nitrogen to C-11 of tomaymycin, rotation of the remaining amino proton that forms one of the Watson–Crick hydrogen bonds between ^{4}G and ^{9}C is restricted, and consequently the normal rate of exchange with D_2O is dramatically reduced. We are able to unambiguously assign by two-dimensional NMR experiments both the orientation (aromatic ring of tomaymycin to the 3′ side of ^{4}G) and covalent linkage stereochemistry (11*S*) of the tomaymycin molecule at the covalent attachment site to ^{4}G of the duplex. Gratifyingly, the conclusion from the proton NMR mea-

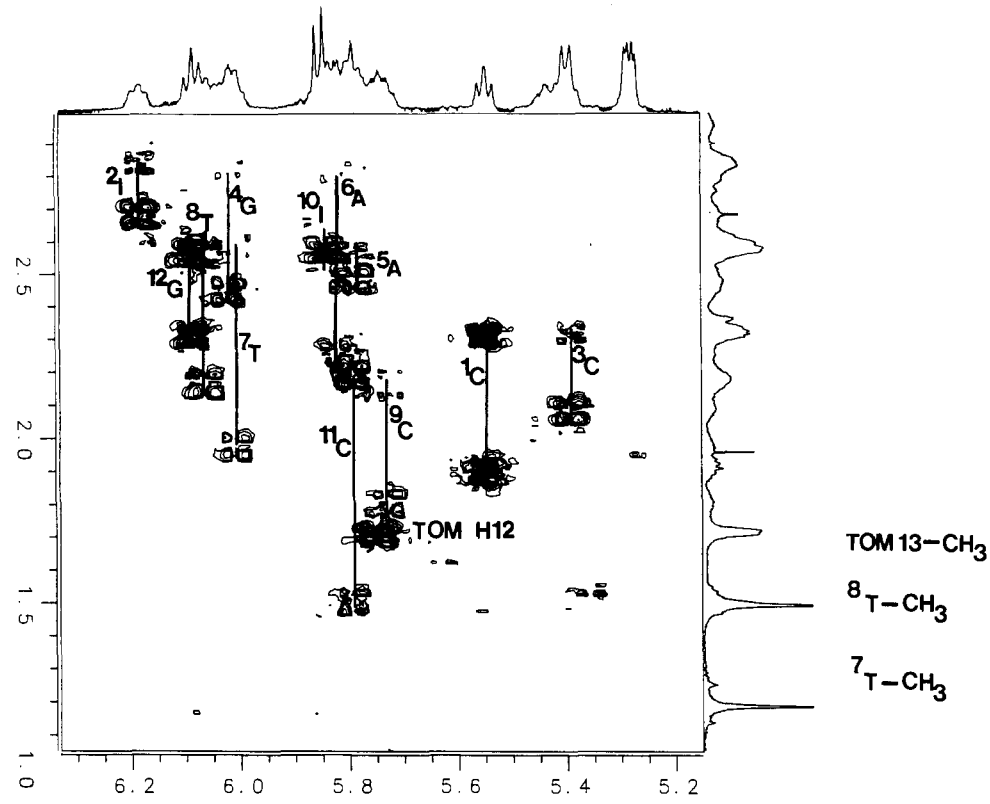

FIGURE 8: Phase-sensitive double quantum filtered COSY expanded contour plot of the H1′ to H2″, H2′ cross peaks for the bis(tomaymycin)–12-mer adduct. Solid lines connect the downfield H2″s to intranucleotide H2′s.

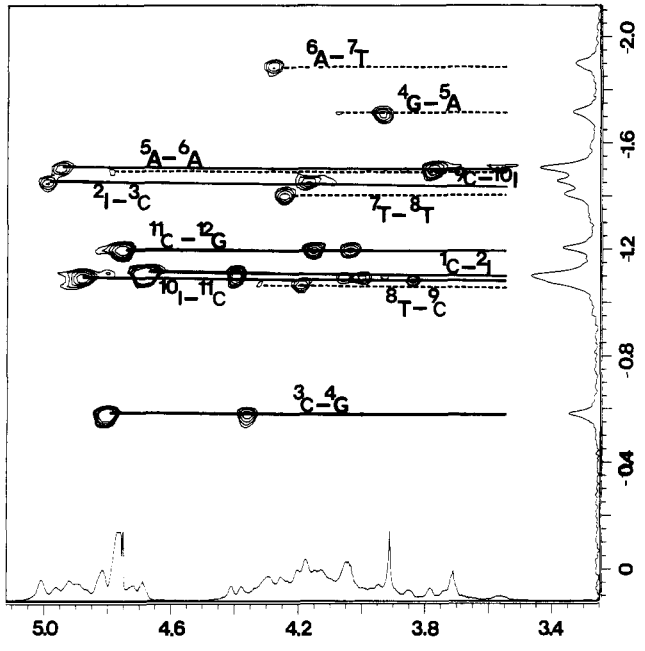

FIGURE 9: Expanded contour plot of the heteronuclear phosphorus-detected phase-sensitive two dimensional ^{31}P–^1H J correlation of the bis(tomaymycin)–12-mer adduct. Solid lines denote definitive assignments. Broken lines denote tentative assignments.

surements concurs with the independent fluorescence assignment of stereochemistry at the covalent linkage site. This substantiates our previous more tentative correlations between fluorescence lifetimes and individual diastereomeric adducts. These were initially made on the basis of fluorescence and NMR correlations of free tomaymycin in protic and aprotic solvents. Thus our previously tentative conclusion of a 65:35 ratio of the (11S,11aS)- and (11R,11aS)-tomaymycin diastereomers on calf thymus DNA (Barkley et al., 1986) and of an approximate 50:50 ratio of the same diasteromers on d(ATGCAT)$_2$ (Cheatham et al., 1988) is now on firm ground.

The energy-minimized structure of the bis(tomaymycin)–d(ClCGAATTClCG)$_2$ adduct having the experimentally determined 11S stereochemistry and 3′ orientation in the minor groove is shown in Figure 10. An overlay of the d(ClCG-AAT·ATTClCG) duplex and the 11S, 3′-oriented tomaymycin–7-mer adduct is shown in Figure 11. Both figures predict minimal distortion of the duplex helix, which is in agreement with the analysis of the two-dimensional COSY and NOESY data (Tables VII and VIII).

Effect of Tomaymycin Covalent Bonding on the Structure of d(ClCGAATTClCG)$_2$. Changes in chemical shifts of deoxynucleotide protons that occur upon tomaymycin modification are mostly restricted to the minor groove in proximity to the drug overlap region, e.g., ^{10}I H2 and ^{4}G H1′ (see Table I). These changes in chemical shifts may be in part due to tomaymycin shielding or deshielding effects. However, oligomer proton chemical shift changes may also reflect a change in nucleotide stacking geometries or a conformational transition (Patel et al., 1987). Two-dimensional spectroscopy results (Tables VII and VIII) confirm changes in the glycosidic angles and sugar geometries for the 12-mer after adduct formation. Comparison of J coupling in Tables VII and VIII shows that two of the most substantial changes in sugar pucker occur at the sites of covalent attachment (^{4}G) and at its 5′-side nucleotide (^{3}C). While these inferences of sugar geometry do not rely on a quantitative measure of proton coupling constants, as for the case of the Dickerson dodecamer (Bax & Lerner, 1988), they do accurately reflect the presence of different furanose geometries. The downfield-shifted ^{3}C–^{4}G phosphorus NMR signal of the bis(tomaymycin) adduct (see Figures 3A,B and 9) also supports the proposed conformational changes at nucleotides ^{3}C and ^{4}G.

A comparison was made of the pseudorotation angles of purine and pyrimidine nucleotides from the X-ray and ^{1}H

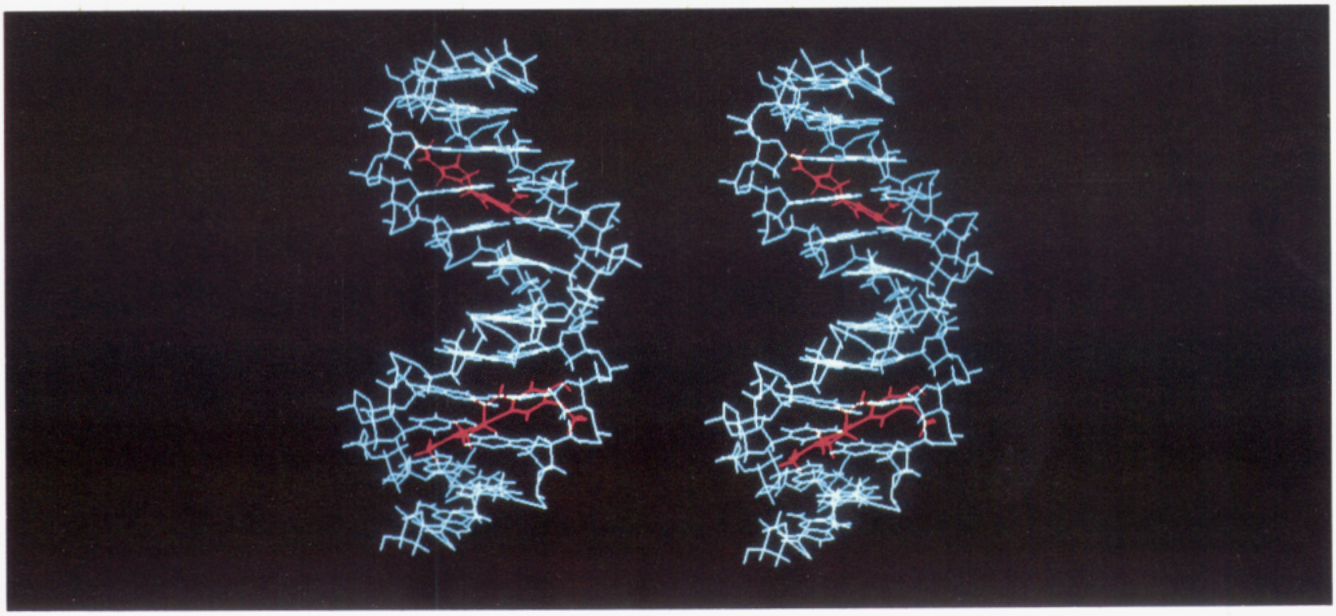

FIGURE 10: Stereo drawing of ^{4}G attached to tomaymycin showing the conformation obtained through minimization with AMBER (see Materials and Methods).

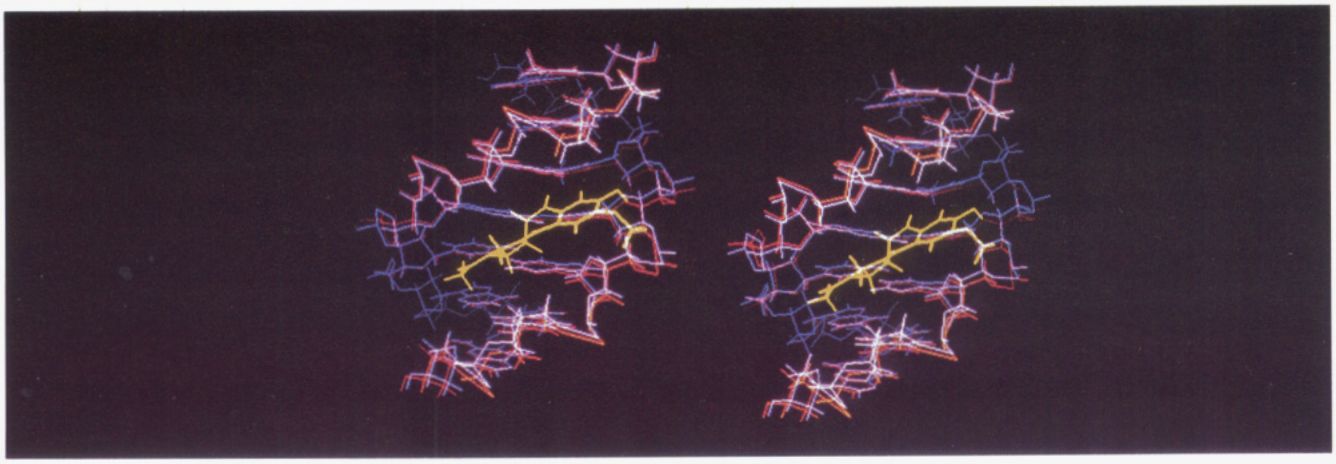

FIGURE 11: Stereo drawing of the superimposed d(CICGAAT·ATTCICG) in orange and tomaymycin–d(CICGAAT·ATTCICG) in magenta and yellow.

NMR data of d(CGCGAATTCGCG)$_2$ (Drew et al., 1981; Bax & Lerner, 1988) and from our proton NMR data of d(CICGAATTCICG)$_2$ and its bis(tomaymycin) adduct (supplementary material). A comparison of the X-ray-determined structure of the Dickerson dodecamer with the solution structure of the inosine-substituted oligomer shows a pseudorotation angle shift from classical B-type toward O1′-endo. This is not without precedent (Chary et al., 1987) and may also be influenced by the substitution of I for G with the accompanying loss of one hydrogen bond for each substitution. Upon formation of the bis(tomaymycin)–12-mer adduct, the population of sugar geometries for the inosine-disubstituted 12-mer shifts back toward C2′-endo. Furthermore, from this analysis, it appears that tomaymycin stabilizes a B-type helical structure after formation of the covalent adduct. Molecular modeling results show less change in sugar geometries of the duplex upon adduct formation, but there is generally agreement between the experimental and theoretical studies.

Relationship between Sequence Selectivity and Apparent Distortion of DNA. It is intriguing that in the anthramycin–d(ATGCAT)$_2$ adduct *two* phosphorus resonances are moved downfield (Boyd et al., 1990), while in the tomaymycin–12-mer duplex adduct only *one* phosphorus resonance is moved downfield. One of these phosphates is common to both the adducts (i.e., that to the 5′ side of the covalently modified guanine) while the other is unique to the anthramycin adduct and is on the 3′ side of guanine on the noncovalently modified strand. If the downfield-shifted phosphorus resonance signals are associated with distortion of the DNA backbone, we can tentatively conclude that upon P(1,4)B adduct formation the anthramycin–d(ATGCAT)$_2$ adduct is more distorted than the bis(tomaymycin)–12-mer adduct. This idea is further supported by unpublished ^{31}P NMR studies on anthramycin bound to an oligomer containing the covalent bonding sequence 5′-AGA-3′. In this case downfield-shifted ^{31}P resonance signals are not observed. Since this oligomer belongs to the most favored P(1,4)B bonding sequence (5′-PuGPu), ^{31}P NMR may be a sensitive tool to evaluate backbone distortion of DNA, as this relates to P(1,4)B preferred sequence selectivity. This suggests a structural rationale for the experimentally determined observation that 5′-PyGPu sequences (i.e., 5′-CGA in the 12-mer) are preferred bonding sites over 5′-PyGPy sequences (i.e., 5′-TGC in the 6-mer) (Hertzberg et al., 1986).

Intermolecular Interactions Determining the Orientation and Stereochemistry of P(1,4)Bs on Different Sequences. The phosphorus and proton NMR results show predominantly (i.e., >90%) one species (11*S*, 3′) of tomaymycin bound to the

Table IX: Patterns for Binding of Tomaymycin with Individual Residues on Polynucleotides[a]

oligonucleotide	confign at C-11	direction	residues[b]											
d(ATGCAT)$_2$	*S*	3′	^{5}S		^{4}S	^{4}S	^{4}C		^{10}C	10,11P	^{11}S	^{11}A	11,12P	^{12}S
d(CICGAAT·ATTCICG)	*S*	3′	^{6}S		^{5}S	^{5}S	^{5}A	^{4}G	^{11}C	11,12P	^{12}S	^{12}I	12,13P	^{13}S
d(ATGCAT)$_2$	*R*	5′	^{5}S	4,5P			^{4}C	^{3}G	^{10}C		^{11}S	^{11}A		^{12}S
d(CICGAAT·ATTCICG)	*R*	5′		5,6P			^{5}A	^{4}G	^{11}C		^{12}S			^{13}S

[a] Only residues that bind to tomaymycin with an energy >−2.0 kcal/mol are included. Residues in CICGAAT·ATTCICG are shifted to one base higher than the corresponding ones in (ATGCAT)$_2$ because of the covalent bonding into ^{4}G in the former and ^{3}G in the latter. [b] S = sugar.

12-mer. This is in contrast to our previously reported results using the d(ATGCAT)$_2$ duplex where two species (11*S*, 3′ and 11*R*, 5′) of tomaymycin were bound in approximately equal amounts (Cheatham et al., 1988). Thus both the orientation in the minor groove and the stereochemistry of tomaymycin bound to DNA are a function of the immediate flanking sequence. For the more preferred bonding sequence (5′-PyGPu) only one species is evident, while the less preferred sequence (5′-PyGPy) shows two species. The species having an 11*S* configuration and 3′ orientation is found on both sequences examined, but the second species having the opposite orientation and stereochemistry at C-11 could not be detected on the more preferred bonding sequence. While molecular modeling using AMBER is in accord with the experimentally determined species for both oligomers, there is a difference in terms of the preferred *pairs of species* that are predicted by modeling; i.e., on d(ATGCAT)$_2$, the two most energetically favored species are the 11*S*, 3′-oriented and 11*R*, 5′-oriented adducts, which differ by 4 kcal/mol (Cheatham et al., 1988), whereas on the 12-mer the two favored species are the 11*S*, 3′-oriented and 11*S*, 5′-oriented adducts, which differ by 2.9 kcal/mol.

The reason for this apparent discrepancy was addressed by examining the calculated interaction energies for tomaymycin and individual polynucleotide residues in each of the species listed in Table IX. Such analyses are complicated because the total binding energies reflect complex binding patterns and a wide distribution of differences in energies between individual residues. However, insight into the effects of binding patterns can be obtained by focusing on the most important interactions—i.e., those of −2.0 kcal/mol or greater energy. Table IX lists the binding patterns for the four species. The construction of this table reflects the increase of *one* in residue numbers in going from ATGCAT to CICGAAT, because of the location of the guanine residues (^{3}G or ^{4}G, respectively) to which the covalent bond is formed. It is evident from this table that the two patterns for the 11*S*, 3′ binding modes are identical, except for the pair ^{3}G–^{4}G, where the interaction is less than −2.0 kcal/mol with d(ATGCAT)$_2$. Even in this case its value of −1.8 kcal/mol is, however, not much less than that of the corresponding interaction for d(CICGAAT·ATTCICG) (−3.6 kcal/mol). A greater contrast occurs in the binding patterns of the two 11*R*, 5′ modes. There are two more interactions between tomaymycin and the polynucleotide residues with d(ATGCAT)$_2$ than with d(CICGAAT·ATTCICG). One of them involves a hydrogen bond, between HN10 of tomaymycin and N3 of ^{11}A, of 1.09-Å length and −5.4 kcal/mol energy. The other is less significant (−2.1 kcal/mol). There is also an unfavorable interaction of +1.7 kcal/mol between O4 of tomaymycin and O3′ of ^{12,13}P in the d(CICGAAT·ATTCICG) sequence. (The O3′ oxygen atom of a sugar is usually considered part of the phosphate to which it also is bonded in AMBER analysis.) This interaction does not occur in the adduct with d(ATGCAT)$_2$. These factors combine to disfavor the 11*R*, 5′ mode for the d(CICGAAT·ATTCICG) sequence as is evident in its relatively poor net binding energy (−10.0 kcal/mol) compared with that of the 11*S*, 3′ mode (−21.2 kcal/mol, Table III). The total distortion energies of these two modes differ by only 3.7 kcal/mol, which means that *binding energies are more important than distortion energies* in favoring the 11*S*, 3′ mode on d(CICGAAT·ATTCICG). Comparable net binding energies for the tomaymycin–d(ATGCAT)$_2$ adducts are −17.9 kcal/mol for the 11*S*, 3′ mode and −21.9 kcal/mol for the 11*R*, 5′ mode. The resulting relatively small difference is consistent with the existence of both binding modes (Cheatham et al., 1988).

In contrast to tomaymycin, when anthramycin is bound to d(ATGCAT)$_2$, only one species of adduct is observed by NMR (Boyd et al., 1990). Solely on the basis of a proton NMR study we could unambiguously assign the 3′ orientation. However, we could not unambiguously differentiate between the 11*R* or 11*S* species bound to this oligomer, because molecular modeling using AMBER predicted scalar coupling between protons at C-11 and C-11a for *both* species. On the basis of energy minimization calculations and interproton cross peaks in the NOESY spectrum, a strong case could be made for 11*S* species.[6] A major difference for the bis(tomaymycin)–12-mer adduct from the anthramycin–d(ATGCAT)$_2$ adduct is the contribution of hydrogen bonding to stabilization of the anthramycin 11*S*, 3′-oriented species. In the anthramycin–d(ATGCAT)$_2$ adduct three hydrogen bonds were identified between the drug and DNA, whereas in the tomaymycin species bound to 5′-CGA the interactions are of the non-hydrogen-bonding varieties. We are presently addressing the question of which molecular interactions between DNA and tomaymycin give rise to the hierarchy of preferred bonding sequences. Thus a comparison of the results of bonding anthramycin or tomaymycin to d(ATGCAT)$_2$ and tomaymycin to the 12-mer leads us to conclude that the orientation and stereochemistry of the drug species bound to DNA are *not only dependent upon sequence but also dependent upon the structure* of the P(1,4)B antibiotic.

Biochemical and Biological Implications. The relatively nondistortive nature of the P(1,4)B–DNA adducts shown in this study and a previous one (Boyd et al., 1990), coupled with the absence of apparent significant changes in electronic or tautomeric characteristics of the covalently modified guanine, raises important questions on how the P(1,4)B–DNA adducts are recognized by repair enzymes. The UVRABC nuclease incision repair complex is able to recognize the anthramycin–DNA adduct and apparently incise both 3′ and 5′ sides

[6] The 11*S*, 3′ species of the anthramycin–d(ATGCAT)$_2$ adduct is favored by about 21 kcal/mol in net binding energies over the 11*R*, 3′ species. The present study on the bis(tomaymycin)–12-mer adduct demonstrates that the 11*S* and 3′-oriented species has a characteristic downfield shift of the proton at C-11 of the P(1,4)B; i.e., this proton is shifted downfield 0.9 ppm relative to the unbound drug. Since such a large downfield shift is *uniquely* associated with the 11*S* species, we tentatively conclude that the stereochemistry of the species of anthramycin bound to d(ATGCAT)$_2$ is also the 11*S*, since in the anthramycin–d(ATGCAT)$_2$ this same resonance signal was also shifted downfield by 1.04 ppm.

of DNA-flanking lesions (Walter et al., 1988). We know from the results reported in this and previous NMR studies on tomaymycin that the stereochemistry at the covalent linkage site and orientation in the minor groove are dependent upon the immediate bonding sequence. This is also true for anthramycin, since on d(GAAGAAC·CTTCTTG) two anthramycin adducts are formed (Boyd, unpublished results). Such observations complicate the overall picture for repair recognition of P(1,4)B–DNA adducts, but these factors must be taken into account if we are to fully understand DNA repair recognition processes.

In both yeast and human cells anthramycin produces double-strand breaks (Hannan & Hurley, 1978; Petrusek et al., 1982). In human cells both the single- and double-strand breaks are persistent and are *repair dependent*, since in XP cells neither single- nor double-strand breaks are detected. This observation coupled with the more recent data on the nondistortive nature of the P(1,4)B adducts raises important questions about whether or not repair incision always takes place on the covalently modified strand.

Conclusions

(1) This study provides the first unequivocal evidence for a covalent adduct between C-11 of a P(1,4)B and the exocyclic 2-amino group of guanine. (2) The species of tomaymycin bound to 5′-CGA has an 11*S* stereochemistry and is oriented with the aromatic ring to the 3′ side of guanine. (3) The minimal distortion produced upon covalent bonding is restricted to the deoxyribose at the covalently modified guanine and the immediate 3′-phosphate and deoxyribose. (4) Tomaymycin appears to stabilize a B-type helical structure. (5) The orientation of a P(1,4)B on DNA and the stereochemistry at the covalent linkage site are dependent upon both the immediate surrounding sequence and the drug structure. (6) Molecular modeling using AMBER is predictive of the orientation and stereochemistry of the P(1,4)Bs on oligodeoxynucleotides and is capable of defining the molecular interactions that favor the different species on various oligomers.

Acknowledgments

We thank Dr. Karol Maskos for performing the fluorescence decay measurements and Joann Haddock for her patience in preparing the manuscript.

Supplementary Material Available

Figure S1 showing the proton NMR spectrum and two-dimensional magnitude COSY of the inosine-disubstituted 12-mer and Figure S2 showing a comparison of the experimentally derived sugar pseudorotation angles for the purine and pyrimidine deoxynucleotides in $d(CGCGAATTCGCG)_2$ from X-ray and ^1H NMR data (4 pages). Ordering information is given on any current masthead page.

References

Arima, K., Kohsaka, M., Tamura, G., Imanaka, M., & Sakai, M. (1972) *J. Antibiot. 24*, 437–444.
Arora, S. (1981) *J. Antibiot. 34*, 462–464.
Barkley, M. D., Cheatham, S., Thurston, D. E., & Hurley, L. H. (1986) *Biochemistry 25*, 3021–3031.
Bax, A., & Sarkar, S. K. (1984) *J. Magn. Reson. 60*, 170–176.
Bax, A., & Lerner, L. (1988) *J. Magn. Reson. 79*, 429–443.
Boyd, F. L., Cheatham, S. F., Remers, W., Hill, G. C., & Hurley, L. H. (1990) *J. Am. Chem. Soc.* (in press).
Chary, K. V. R., Hosur, R. V., Govie, G., Zu-Kun, T., & Miles, H. T. (1987) *Biochemistry 26*, 1315–1322.
Cheatham, S. F., Kook, A. M., Hurley, L. H., Barkley, M. D., & Remers, W. (1988) *J. Med. Chem. 31*, 583–590.
Drew, H. R., Wing, R. M., Takano, T., Broka, C., Tanaka, S., Itakura, K., & Dickerson, R. E. (1981) *Proc. Natl. Acad. Sci. U.S.A. 78*, 2179–2183.
Ferrin, T. E., Huang, C. C., Jarvis, L. E., & Langridge, R. (1988a) *J. Mol. Graphics 6*, 1–12.
Ferrin, T. E., Huang, C. C., Jarvis, L. E., & Langridge, R. (1988b) *J. Mol. Graphics 6*, 13–27.
Goa, X., & Patel, D. J. (1989) *Biochemistry 28*, 751–762.
Graves, D. E., Pattaroni, C., Krishnan, B. S., Ostrander, J. M., Hurley, L. H., & Krugh, T. R. (1984) *J. Biol. Chem. 259*, 8202–8209.
Graves, D. E., Stone, M. P., & Krugh, T. R. (1985) *Biochemistry 24*, 7573–7581.
Haasnoot, C. A. G., Westerink, H. P., van der Marel, G. A., & van Boom, J. H. (1984) *J. Biomol. Struct. Dyn. 2*, 345–360.
Hannan, M., & Hurley, L. H. (1978) *J. Antibiot. 31*, 911–913.
Hare, D. R., Wemmer, D. E., Chou, S. H., Drobay, G., & Reid, B. R. (1983) *J. Mol. Biol. 171*, 319–336.
Hertzberg, R. P., Hecht, S. M., Reynolds, V. L., Molineux, I. J., & Hurley, L. H. (1986) *Biochemistry 25*, 1249–1258.
Hore, P. J. (1983) *J. Magn. Reson. 55*, 283–300.
Hosur, R. V., Ravikumar, M., Chary, K. V. R., Sheth, A., Govil, G., Zu-Kun, T., & Miles, H. T. (1986) *FEBS Lett. 205*, 71–76.
Hurley, L. H. (1977) *J. Antibiot. 30*, 349–370.
Hurley, L. H., & Petrusek, R. (1979) *Nature 282*, 529–530.
Hurley, L. H., & Needham-VanDevanter, D. (1986) *Acc. Chem. Res. 13*, 263–269.
Hurley, L. H., Reck, T., Thurston, D. E., Holden, K. G., Hertzberg, R. P., Hoover, J. R. E., Gallagher, G., Faucette, L. F., Jr., Mong, S.-M., & Johnson, R. K. (1988) *Chem. Res. Toxicol. 1*, 258–268.
Knutson, J. R., Beechem, J. M., & Brand, L. (1983) *Chem. Phys. Lett. 102*, 501–507.
Kolber, Z. S., & Barkley, M. D. (1986) *Anal. Biochem. 152*, 6–21.
Kumar, R. M., Hosur, R. V., Roy, K. B., Miles, H. T., & Govil, G. (1985) *Biochemistry 24*, 7703–7711.
Mostad, A., Romming, C., & Storm, B. (1978) *Acta Chem. Scand., Ser. B 32*, 639–648.
Patel, D. J., Shapiro, L., & Hare, D. (1987) *Q. Rev. Biophys. 20*, 35–112.
Petrusek, R. L., Anderson, G. L., Garner, T. F., Fannin, Q. L., Kaplan, D. J., Zimmer, S. G., & Hurley, L. H. (1981) *Biochemistry 20*, 1111–1119.
Petrusek, R. L., Uhlenhopp, E. L., Duteau, N., & Hurley, L. H. (1982) *J. Biol. Chem. 257*, 6207–6216.
Rao, S. N., Singh, U. C., & Kollman, P. A. (1986) *J. Med. Chem. 29*, 2484–2492.
Reid, B. R. (1987) *Q. Rev. Biophys. 20*, 1–34.
Remers, W. A. (1988) in *The Chemistry of Antitumor Antibiotics*, Vol. 2, pp 28–92, John Wiley & Sons, New York.
Remers, W. A., Mabilia, M., & Hopfinger A. J. (1986) *J. Med. Chem. 29*, 2492–2503.
States, D. J., Haberkorn, R. A., & Ruben, D. J. (1982) *J. Magn. Reson. 48*, 286.
Thurston, D. E., & Hurley, L. H. (1984) *Drug Future (CIPS) 8*, 957–971.
Walter, R. B., Pierce, J., Case, R., & Tang, M.-S. (1988) *J. Mol. Biol. 203*, 939–947.
Weiner, P. K., & Kollman, P. A. (1984) *J. Comput. Chem.*

2, 287-303.
Weiner, S. J., Kollman, P. A., Case, D., Singh, U. C., Ghio, C., Alagona, G., Profeta, S., Jr., & Weiner, P. K. (1984) J. Am. Chem. Soc. 106, 765-784.
Zakrzewska, K., & Pullman, B. (1986) J. Biomol. Struct. Dyn. 4, 127-136.

pH-Induced Denaturation of Proteins: A Single Salt Bridge Contributes 3-5 kcal/mol to the Free Energy of Folding of T4 Lysozyme

D. Eric Anderson, Wayne J. Becktel, and F. W. Dahlquist*
Institute of Molecular Biology and Department of Chemistry, University of Oregon, Eugene, Oregon 97403
Received August 29, 1989; Revised Manuscript Received November 1, 1989

ABSTRACT: The energetics of a salt bridge formed between the side chains of aspartic acid 70 (Asp70) and histidine 31 (His31) of T4 lysozyme have been examined by nuclear magnetic resonance techniques. The pK_a values of the residues in the native state are perturbed from their values in the unfolded protein such that His31 has a pK_a value of 9.1 in the native state and 6.8 in the unfolded state at 10 °C in moderate salt. Similarly, the aspartate pK_a is shifted to a value of about 0.5 in the native state from its value of 3.5-4.0 in the unfolded state. These shifts in pK_a show that the salt bridge is stabilized 3-5 kcal/mol. This implies that the salt bridge stabilizes the native state by 3-5 kcal/mol as compared to the unfolded state. This is reflected in the thermodynamic stability of mutants of the protein in which Asp70, His31, or both are replaced by asparagine. These observations and consideration of the thermodynamic coupling of protonation state to folding of proteins suggest a mechanism of acid denaturation in which the unfolded state is progressively stabilized by protonation of its acid residues as pH is lowered below pH 4. The unfolded state is stabilized only if acidic groups in the folded state have lower pK_a values than in the unfolded state. When the pH is sufficiently low, the acid groups of both the native and unfolded states are fully protonated, and the apparent unfolding equilibrium constant becomes pH independent. Similar arguments apply to base-induced unfolding. These observations suggest that the electrostatic contribution of each ionizable group to the stability of the folded state can be directly assessed by simply measuring its apparent pK_a by NMR or other methods.

The pH dependence of the thermodynamic stability of proteins has long been of interest to biochemists. Linderström-Lang (1924) was one of the first to suggest a plausible reason for the lowered stability of proteins at extremes of pH. In this view, the stability was determined by electrostatic interactions in the native, folded state of a protein. For example, at acidic pH, the decreased stability would be the result of unfavorable electrostatic interactions introduced by the increase in positive charge on a protein. Similar arguments accounted for the decrease in stability observed in highly basic solutions due to repulsion of negative charges. The theory predicted maximum stability at or near the isoelectric point of the protein where the net charge is zero. This model has been extended to include more detailed considerations of charge–charge interactions of the native state (Matthews & Gurd, 1986).

A number of proteins, with acidic or basic isoelectric points, are observed to have maximal thermodynamic stability near neutrality. This observation suggests that considerations in addition to overall charge are important in determining the contribution of ionizable groups to the overall folding energy of globular proteins. For example, the lysozyme produced by the bacteriophage T4 is a rather basic protein with an isoelectric point above pH 10 yet is most stable near pH 5. This genetically manipulable, 164-residue protein without disulfide bonds has been the object of intense structural [Matthews & Remington, 1974; Matsumura et al. (1988) and Nicholson et al. (1988) and references cited therein], thermodynamic (Hawkes et al., 1984; Becktel & Baase, 1987; Becktel & Schellman, 1987), and spectroscopic (McIntosh et al., 1987a,b) investigation and provides an excellent model protein in which to study interactions between ionizable residues and protein stability.

Materials and Methods

Site-directed mutagenesis (Zoeller & Smith, 1983) was performed essentially as described by Kunkel (1985) on M13 single-strand DNA containing a derivative of the T4 lysozyme gene in which codons for cysteine residues 54 and 97 had been changed to encode threonine and alanine, respectively [Matsumara et al. (1988) and references cited therein]. Directed mutations were H31N, D70E, D70N, and H31N/D70N. Mutations were confirmed by chain-termination dideoxy sequencing (Sanger et al., 1977). T4 lysozyme was produced and specifically enriched in [4-^{13}C]aspartic acid (99%, Merck Sharp & Dohme of Canada) according to an approach described elsewhere (Muchmore et al., 1989). Reversible unfolding of T4 lysozymes was monitored with the change in dichroism at 223 nm, as has been described (Elwell & Schellman, 1977; Becktel & Baase, 1987).

For histidine titrations of the folded state, the protein was transferred to a D_2O buffer of 10 mM D_3PO_4 and 10 mM KCl, heated to 55 °C for 0.5 h, and slowly cooled. This treatment reversibly unfolds the protein and allows rapid exchange of all amide protons by deuterons. After refolding, the protein retains its enzymatic activity and appears to be otherwise identical with the native protein before exchange.

All titrations and pH measurements were performed at 10 °C. Proton NMR measurements of the pH dependence of

* To whom correspondence should be addressed.

0006-2960/90/0429-2403$02.50/0